Spin structure of harmonically trapped one-dimensional atoms with spin-orbit coupling

Q. Guan and D. Blume

Spin structure of harmonically trapped one-dimensional atoms with spin-orbit coupling

Q. Guan[1] and D. Blume[1]

[1]Department of Physics and Astronomy, Washington State University, Pullman, Washington 99164-2814, USA

We introduce a theoretical approach to determine the spin structure of harmonically trapped atoms with two-body zero-range interactions subject to an equal mixture of Rashba and Dresselhaus spin-orbit coupling created through Raman coupling of atomic hyperfine states. The spin structure of bosonic and fermionic two-particle systems with finite and infinite two-body interaction strength g is calculated. Taking advantage of the fact that the N-boson and N-fermion systems with infinitely large coupling strength g are analytically solvable for vanishing spin-orbit coupling strength k_{so} and vanishing Raman coupling strength Ω, we develop an effective spin model that is accurate to second-order in Ω for any k_{so} and infinite g. The three- and four-particle systems are considered explicitly. It is shown that the effective spin Hamiltonian, which contains a Heisenberg exchange term and an anisotropic Dzyaloshinskii-Moriya exchange term, describes the transitions that these systems undergo with the change of k_{so} as a competition between independent spin dynamics and nearest-neighbor spin interactions.

PACS numbers:

I. INTRODUCTION

Spin-orbit (more precisely, spin-momentum) coupled systems continue to attract a great deal of attention due to the rich physics of the spin-Hall effect, topological insulators, and Majorana fermions [1–5]. While these topics fall traditionally into condensed matter territory, recent advances in cold atomic gases have led to a fruitful cross fertilization of atomic and condensed matter physics. On the experimental side, synthetic gauge fields have been realized in ultracold atom systems [6–15]. On the theoretical side, systems with different kinds of spin-orbit coupling have been studied at the many- and few-body levels [6, 16–24]. Understanding the effects of spin-orbit coupling in few-atom systems opens the door to a bottom-up understanding of many-body systems. Nowadays, ultracold few-atom systems can be prepared and manipulated in experiments [25, 26]. For example, taking advantage of a Fano-Feshbach resonance, the interaction between the atoms can be tuned [27]. Moreover, the confinement geometry can be changed from three-dimensional to effectively two-dimensional to effectively one-dimensional [28]. These experimental advances were guided by and stimulated a good number of theoretical few-body studies [29–42]. Much analytical work has been done by approximating the true alkali atom-alkali atom potential by a zero-range contact potential [29, 32–34, 36, 40–45]. This approximation captures the low energy regime reliably but fails to reproduce high-energy properties (such as the characteristics of deeply bound states). Assuming zero-range interactions, the energy spectra of two one-dimensional bosons and two one-dimensional fermions with arbitrary two-body coupling constant and spin-orbit coupling strength have been calculated and the interplay between the spin-orbit coupling term, Raman coupling term, and the two-body potential has been analyzed [20].

Extending earlier work [20, 21], this paper investi-gates the spin structure of harmonically trapped atoms with two-body zero-range interactions subject to an equal mixture of Rashba and Dresselhaus spin-orbit coupling created through Raman coupling of atomic hyperfine states. The spin structure of two identical one-dimensional bosons and two identical one-dimensional fermions with finite and infinite two-body interaction strength g is calculated for weak to strong spin-orbit coupling strength. The bosonic and fermionic systems display, in general, different behaviors as the spin-orbit coupling strength k_{so} and the two-body coupling constant g are changed. For infinite g, however, the bosonic and fermionic systems display the same spin structure. An interesting transition of the spin structure is found in going from small to large k_{so}. To understand the system behaviors for finite and infinite g, an effective Hamiltonian for any k_{so} that is accurate up to second order in the Raman coupling strength Ω is derived. Effective Hamiltonian have been utilized in various areas of physics and the Hubbard model [46], the Born-Oppenheimer approximation [47], the Ising model [48], and the Heisenberg spin chain [49] are prominent examples. Various approaches to generate effective Hamiltonian and the connection between perturbation theory and selected effective Hamiltonian have been discussed in Refs. [50–55].

For infinitely large g and arbitrary N, we integrate out the spatial degrees of freedom and recast the resulting effective Hamiltonian in terms of spin operators. Single spin terms are proportional to Ω while spin-spin interactions are proportional to Ω^2. Effective spin Hamiltonian have been derived previously for one-dimensional systems without spin-orbit and Raman coupling [56–59]. In those cases, spin-spin interactions were introduced by allowing for small deviations from $|g| = \infty$; in essence, this introduces a tunneling term. In our case, the single spin and the spin-spin terms are introduced by the Raman coupling. The single spin term is proportional to Ω and has been discussed in Ref. [21]. In essence, the Raman

coupling creates an effective local $\vec{B}$-field that the spins follow. The spin-spin interaction term has, to the best of our knowledge, not been discussed before in this context. This term contains two contributions. The first contribution is of the type of the "usual" Heisenberg exchange term [45], i.e., it is a $\vec{\sigma}_j \cdot \vec{\sigma}_k$ term, where $\vec{\sigma}_j$ is the spin operator of spin j. The second contribution is of the type of the anisotropic Dzyaloshinskii-Moriya exchange term, i.e., it is a one-dimensional analog of the $\vec{D} \cdot (\vec{\sigma}_j \times \vec{\sigma}_k)$ term [60–62], where $\vec{D}$ is a constant vector.

The remainder of this paper is organized as follows: Section II defines the system Hamiltonian, discusses its symmetries and introduces an effective low-energy Hamiltonian. Section III determines the spin structure of the two-particle system for different g and k_{so}. Using the effective low-energy Hamiltonian, Sec. IV derives an effective spin Hamiltonian for infinitely large g and applies this Hamiltonian to determine the spin correlations of the three- and four-particle systems. A transition from a regime where the dynamics is governed by single spin physics to a regime where the dynamics is governed by spin-spin interactions is obtained. Finally, Sec. V summarizes and concludes. The appendices contain a number of technical details, including the evaluation of the matrix elements for infinite g, which are needed to construct both the effective Hamiltonian and the full Hamiltonian. The analytical techniques and results are expected to be useful for other one-dimensional studies.

II. SYSTEM HAMILTONIAN AND GENERAL CONSIDERATIONS

We consider N one-dimensional atoms of mass m in a harmonic trap with angular trapping frequency ω and zero-range two-body interactions $g\delta(x_j - x_k)$, where x_j is the position of the jth particle with respect to the center of the trap. We assume that each particle feels an equal mixture of Rashba and Dresselhaus spin-orbit coupling of strength k_{so} and Raman coupling of strength Ω. The system Hamiltonian $\tilde{H}$ reads

$$\tilde{H} = H_{sr}\hat{I} + \sum_{j=1}^{N} \frac{\hbar k_{so}}{m}p_j\sigma_y^{(j)} + \frac{\Omega}{2}\sigma_x^{(j)}, \qquad (1)$$

where

$$H_{sr} = \sum_{j=1}^{N} -\frac{\hbar^2}{2m}\frac{\partial^2}{\partial x_j^2} + \frac{1}{2}m\omega^2 x_j^2 + \sum_{j<k} g\delta(x_j - x_k). \quad (2)$$

In Eq. (1), $\hat{I}$ is the 2×2 identity matrix, $\sigma_x^{(j)}$ and $\sigma_y^{(j)}$ are spin-1/2 Pauli matrices of the jth particle, and p_j is the momentum operator of the jth particle along the x-direction. Our goal in the following is to determine the eigenstates $\tilde{\Psi}$ and eigenenergies $\tilde{E}$ of $\tilde{H}$.

To this end, we perform a unitary transformation and define $H = U^\dagger \tilde{H} U$, where $U = \Pi_{j=1}^{N} \exp(-ik_{so}x_j\sigma_y^{(j)})$.

The transformed Hamiltonian H reads

$$H = H_0\hat{I} + \frac{\Omega}{2}V_R \qquad (3)$$

with

$$H_0 = H_{sr} - \frac{N\hbar^2 k_{so}^2}{2m} \qquad (4)$$

and

$$V_R = \sum_{j=1}^{N} \exp(ik_{so}x_j\sigma_y^{(j)})\sigma_x^{(j)}\exp(-ik_{so}x_j\sigma_y^{(j)}). \quad (5)$$

The eigenvalues of H are the same as those of $\tilde{H}$ while the eigenstates Ψ of H are related to the eigenstates $\tilde{\Psi}$ of $\tilde{H}$ by $\Psi = U\tilde{\Psi}$. Our strategy for solving the Schrödinger equation $H\Psi = E\Psi$ is as follows: We first find the eigenstates of H_0 and $H_0\hat{I}$ and then account for the Raman coupling term V_R through either a matrix diagonalization or an effective low-energy Hamiltonian approach that is accurate to second order in Ω.

We denote the eigenstates and eigenenergies of H_{sr} by $\phi_n(\vec{x})$ and E_n, where n collectively denotes the quantum numbers needed to label the states and $\vec{x}$ collectively denotes the N spatial degrees of freedom, $\vec{x} = (x_1, x_2, \cdots, x_N)$. In general, the $\phi_n(\vec{x})$ are not known. Since H_0 is independent of spin, the eigenstates of $H_0\hat{I}$ can be written as

$$\psi_{n,s_1,s_2,\cdots,s_N} = \phi_n(\vec{x})|s_1, s_2, \cdots, s_N\rangle_y, \qquad (6)$$

where the $|s_1, s_2, \cdots, s_N\rangle_y$ are eigenstates of the operator $\sigma_y = \sum_{j=1}^{N} \sigma_y^{(j)}$, i.e., $\sigma_y^{(j)}|s_j\rangle_y = s_j|s_j\rangle_y$ with $s_j = \pm 1$. The eigenenergies of these eigenstates are $E_n - N\hbar^2 k_{so}^2/(2m)$. The eigenstates with the same $\phi_n(\vec{x})$ but different spin configurations are degenerate. Thus one can form linear combinations of the $\psi_{n,s_1,s_2,\cdots,s_N}$ such that the resulting eigenstates are eigenstates of the $\vec{\sigma}^2$ operator, where $\vec{\sigma}^2 = (\sum_{j=1}^{N} \vec{\sigma}^{(j)})^2$. For non-vanishing Ω, H no longer commutes with σ_y or $\vec{\sigma}^2$, implying that the total spin and the total projection quantum numbers are no longer conserved. However, H still contains symmetries. Specifically, H commutes with all P_{jk} ($j, k = 1, ..., N$) operators and the Y operator. P_{jk} exchanges both the spatial and spin coordinates of particles j and k. It follows that the eigenstates of H can be classified according to whether or not they change sign under the P_{jk} operator. Throughout this paper, we restrict ourselves to the N identical boson and N identical fermion sectors. The operator Y can be written as $\Pi_{j=1}^{N} Q_j \bigotimes \sigma_x^{(j)}$, where Q_j changes the sign of the spatial coordinate of particle j. It follows that the eigenstates of H, which are also eigenstates of Y, always include an equal mixture of $|s_1, s_2, \cdots, s_N\rangle_y$ and $|\bar{s}_1, \bar{s}_2, \cdots, \bar{s}_N\rangle_y$, where $|\bar{s}_j\rangle_y$ denotes the state obtained by operating with $\sigma_x^{(j)}$ onto $|s_j\rangle_y$. Correspondingly, the expectation value of σ_y, and thus S_y, is always zero. We label the symmetries of the eigenstates by (a, b), where $(a, b) = (1, 1), (1, -1), (-1, 1)$, and

$(-1, -1)$ indicate bosonic ($a = 1$) or fermionic symmetry ($a = -1$) with positive ($b = 1$) or negative ($b = -1$) eigenvalue of Y.

In what follows, we are interested in the expectation values of the local spins $S_x(x)$ and $S_z(x)$ in the x- and z-directions,

$$S_x(x) = \sum_{j=1}^{N} \frac{\hbar}{2} \sigma_x^{(j)} \delta(x - x_j) \qquad (7)$$

and

$$S_z(x) = \sum_{j=1}^{N} \frac{\hbar}{2} \sigma_z^{(j)} \delta(x - x_j). \qquad (8)$$

As already mentioned, we have $\langle S_y(x) \rangle = 0$. To quantify the correlations of the system, we define the projector $P_{|M_s|=m}$,

$$P_{|M_s|=m} = \sum_{|M_s|=m} |s_1, s_2, \cdots, s_N\rangle_{yy} \langle s_1, s_2, \cdots, s_N|, \qquad (9)$$

where M_s is the spin projection quantum number in the y-direction, $M_s = s_1 + s_2 + \cdots + s_N$. The expectation value of $P_{|M_s|=m}$ yields the probability to find the system in the space spanned by all the states with the same absolute value of M_s. For example, for the three particle system, $M_s = \pm 1$ and ± 3. In this case, $P_{|M_s|=1}$ and $P_{|M_s|=3}$ measure the configurations with $M_s = \pm 1$ and $M_s = \pm 3$, respectively.

To diagonalize H directly, we start with the eigenstates of $H_0 \hat{I}$ [see Eq. (6)]. By taking appropriate linear combinations of $\psi_{n,s_1,s_2,\cdots,s_N}$, the Hamiltonian matrix for the different (a, b) symmetry channels can be set up and diagonalized separately. The off-diagonal matrix elements of H contain spatial integrals of the form $(\Omega/2) \int_{-\infty}^{\infty} \phi_n^*(\vec{x}) \phi_m(\vec{x}) e^{\pm 2ik_{so}x_j} d\vec{x}$, which is the Fourier

transform with respect to the coordinate x_j of the product of two eigenstates of H_0. As discussed in Appendix A, these integrals can be evaluated up to any precision numerically and in some cases can be calculated fully analytically.

Since we are primarily interested in the lowest eigenenergy and eigenstate of H for non-zero Ω, we derive an effective low-energy Hamiltonian, which describes much of the system dynamics accurately and is numerically more tractable. The idea is to divide the Hilbert space spanned by $H_0 \hat{I}$ into two pieces called H_L and H_H [54, 55]. The low-energy space H_L contains the eigenstates with energy less than a preset value and the high-energy space H_H contains the eigenstates with energy larger than this preset value. The eigenstates of the effective Hamiltonian H_{eff}, which accounts for the Raman coupling term $(\Omega/2)V_R$ perturbatively, are linear combinations of the unperturbed states of $H_0 \hat{I}$ that lie in H_L. We write

$$H_{eff} = H_{eff}^{(0)} + H_{eff}^{(1)} + H_{eff}^{(2)}, \qquad (10)$$

where

$$H_{eff}^{(m)} = \sum_{\substack{s_1, s_2, \cdots, s_N \\ s_1', s_2', \cdots, s_N' \\ l_j, l_k \in H_L}} |\psi_{l_j, s_1, s_2, \cdots, s_N}\rangle \times$$

$$\langle \psi_{l_j, s_1, s_2, \cdots, s_N} | A_{l_j l_k}^{(m)} | \psi_{l_k, s_1', s_2', \cdots, s_N'} \rangle \langle \psi_{l_k, s_1', s_2', \cdots, s_N'} | \qquad (11)$$

with

$$A_{l_j l_k}^{(0)} = H_0, \qquad (12)$$

$$A_{l_j l_k}^{(1)} = \frac{\Omega}{2} V_R, \qquad (13)$$

and

$$A_{l_j l_k}^{(2)} = \frac{\Omega^2}{8} \sum_{\substack{s_1'', s_2'', \cdots, s_N'' \\ h_n \in H_H}} \left(\frac{V_R |\psi_{h_n, s_1'', s_2'', \cdots, s_N''}\rangle \langle \psi_{h_n, s_1'', s_2'', \cdots, s_N''} | V_R}{E_{l_j} - E_{h_n}} + \frac{V_R |\psi_{h_n, s_1'', s_2'', \cdots, s_N''}\rangle \langle \psi_{h_n, s_1'', s_2'', \cdots, s_N''} | V_R}{E_{l_k} - E_{h_n}} \right). \qquad (14)$$

An important point is that the second-order term $A_{l_j l_k}^{(2)}$ runs over all states from the H_H Hilbert space. In essence, this leads to a renormalization of the matrix elements in the low-energy space H_L.

To obtain an intuitive understanding of the effective Hamiltonian approach, Figs. 1(a) and 1(b) show the single-particle momentum space potentials ($p \pm \hbar k_{so})^2/(2m)$ for $k_{so} a_{ho} = 2$ and $k_{so} a_{ho} = 4$, respectively. In this picture, the potentials centered at $p = -\hbar k_{so}$

and $p = \hbar k_{so}$ are occupied by the spin-up and spin-down components of the wave function. The Raman coupling term introduces a mixing of the spin-up and spin-down potentials. Within the effective Hamiltonian approach, this is accounted for by $H_{eff}^{(1)}$ and $H_{eff}^{(2)}$. To estimate the relative importance of $H_{eff}^{(1)}$ and $H_{eff}^{(2)}$, we consider the $g = \infty$ case (this case is discussed in detail in Sec. IV). For $g = \infty$, the N-particle wave functions are constructed from the non-interacting single-particle harmonic oscilla-
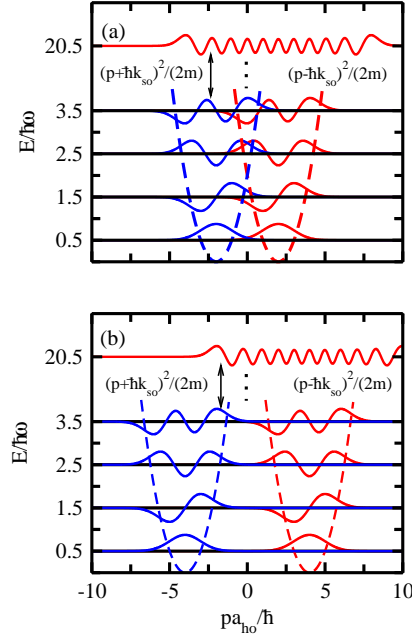
FIG. 1: (Color online) Single-particle momentum space potentials $(p \pm \hbar k_{so})^2/(2m)$ (dashed lines) and non-interacting single-particle momentum space wave functions (solid lines) for (a) $k_{so}a_{ho} = 2$ and (b) $k_{so}a_{ho} = 4$, respectively. The potential and wavefunctions centered at $p = -\hbar k_{so}$ are for the spin-up component and those centered at $p = \hbar k_{so}$ are for the spin-down component. For small k_{so}, the spin-up and spin-down single-particle wavefunctions in the Hilbert space H_L (here, states with $E \le 3.5\hbar\omega$) have overlap, indicating that the first-order effective Hamiltonian dominates. For large k_{so}, the spin-up and spin-down single particle wavefunctions in the Hilbert space H_L have essentially zero overlap, indicating that coupling to highly excited states is dominant, leading to a dominant second-order effective Hamiltonian.

tor states. For $N = 4$, e.g., the single-particle states shown in Figs. 1(a) and 1(b) contribute. The Hamiltonian $H_{eff}^{(1)}$ couples states centered at $p = -\hbar k_{so}$ and $\hbar k_{so}$. Visually, it is clear that the coupling (i.e., the overlap between the different single-particle states centered at $p = -\hbar k_{so}$ and $\hbar k_{so}$) decreases with increasing k_{so}. As a consequence, the Hamiltonian term $H_{eff}^{(2)}$ may carry a higher "weight" than $H_{eff}^{(1)}$ for sufficiently large k_{so} despite the fact that $H_{eff}^{(2)}$ is suppressed by the factor $\Omega/(\hbar\omega)$ for $\Omega < \hbar\omega$. More quantitatively, the Nth single-particle state is distributed in the momentum interval $(\pm\hbar k_{so} - \hbar k_F, \pm\hbar k_{so} + \hbar k_F)$, where $k_F a_{ho} \sim \sqrt{2N}$. Thus for $k_{so} \ge \sqrt{2N}/a_{ho}$, the coupling matrix elements entering into $H_{eff}^{(1)}$ are expected to be small while the coupling matrix elements entering into $H_{eff}^{(2)}$ are expected to have a comparatively large amplitude [the vertical arrow in Figs. 1(a) and 1(b) indicates the momentum region where the Nth single-particle state overlaps with a highly excited single-particle state]. Our pictorial analysis is confirmed by our quantitative calculations. Specifically, as detailed in Sec. IV B, the spin structure changes dramatically at a critical k_{so} value, beyond which the term $H_{eff}^{(2)}$ dominates over the term $H_{eff}^{(1)}$. Analogous arguments can be made for finite g.

Based on the effective Hamiltonian given in Eq. (10),

the next section calculates the spin structure for two-particle systems with arbitrary coupling constant g and compares the results with those obtained from the full ("brute force") diagonalization.

III. TWO-PARTICLE SYSTEM WITH ARBITRARY g

For the two-particle system, the Schrödinger equation for H_{sr} has been solved analytically for arbitrary two-body interaction strength in the literature [29]. The eigenstates are $\phi_n(\vec{x}) = \Phi_p(R)\varphi_q(r)$ with eigenenergy $E_n = (p + 2q + 1)\hbar\omega$, where the center of mass coordinate R and the relative coordinate r are defined through $R = (x_1 + x_2)/\sqrt{2}$ and $r = (x_1 - x_2)/\sqrt{2}$. The center of mass eigenstates $\Phi_p(R)$ are the harmonic oscillator eigenstates with energy $(p + 1/2)\hbar\omega$, where $p = 0, 1, \cdots$. For states with even parity in the relative coordinate, the relative eigenstates $\varphi_q(r)$ are given by $N_q U(-q, 1/2, (r/a_{ho})^2) \exp[-r^2/(2a_{ho}^2)]$, where a_{ho} denotes the harmonic oscillator length,

$$a_{ho} = \sqrt{\frac{\hbar}{m\omega}}, \qquad (15)$$

N_q is a normalization constant and U is the confluent hypergeometric function. In this even parity case, q denotes

a non-integer quantum number, which is determined by the transcendental equation [29]

$$\frac{2\Gamma(-q+1/2)}{\Gamma(-q)} = -\frac{g}{\sqrt{2}\hbar\omega a_{ho}}. \quad (16)$$

For states with odd parity in the relative coordinate, the relative eigenstates $\varphi_q(r)$ are again harmonic oscillator eigenstates with eigenenergy $(2q+1/2)\hbar\omega$, where q takes half-integer values, i.e., $q = 1/2, 3/2, \cdots$. Since the two-body δ-function only acts at $r = 0$, the odd-parity eigenstates and eigenenergies are independent of g. The eigenenergies of the even-parity relative eigenstates, in contrast, change with g. Specifically, the energy $(2q+1/2)\hbar\omega$ increases with increasing g. For infinite g, the ground state of the two-particle system is doubly degenerate, i.e., the relative energies of the even-parity state and the odd-parity state coincide, yielding a total energy of $2\hbar\omega$. This degeneracy plays, as we show below, an important role when the spin-orbit and Raman coupling strengths are non-zero.

When k_{so} and Ω are non-zero, the center of mass and relative degrees of freedom are coupled. In order to describe the interplay between the two-body interaction and the Raman and spin-orbit couplings, the states with spatial parts $\Phi_0(R)\varphi_{q_0}(r)$ and $\Phi_0(R)\varphi_{q_1}(r)$ span the H_L space. Here φ_{q_0} and φ_{q_1} denote the energetically lowest-lying relative even-parity and odd-parity states, respectively. We choose the spatial basis functions to be real. Our motivation for choosing this H_L space is as follows. We want the resulting effective low-energy Hamiltonian to describe the ground state of the two-particle system with good accuracy for all g. For small g, e.g., the low-energy Hamiltonian constructed using $\Phi_0(R)\varphi_{q_0}(r)$ would suffice since the energy of the state $\Phi_0(R)\varphi_{q_1}(r)$ is close to $\hbar\omega$ higher in energy. Including this state in H_L changes the effective low-energy Hamiltonian and its resulting eigenenergies negligibly. For large g, in contrast, the state $\Phi_0(R)\varphi_{q_1}(r)$ needs to be included in H_L since its energy is, as discussed above, nearly degenerate with the state $\Phi_0(R)\varphi_{q_0}(r)$. Thus, the space H_L identified above is the minimal space needed if an effective description of the ground state for all g (small and large) is sought.

For two identical bosons, the ground state ψ_{gr}^b of the effective Hamiltonian H_{eff} is

$$\psi_{gr}^b = \frac{C_1^b}{\sqrt{2}}\Phi_0(R)\varphi_{q_0}(r)(|\uparrow\uparrow\rangle_y + |\downarrow\downarrow\rangle_y)$$

$$+\frac{C_2^b}{\sqrt{2}}\Phi_0(R)\varphi_{q_0}(r)(|\uparrow\downarrow\rangle_y + |\downarrow\uparrow\rangle_y)$$

$$+\frac{C_3^b}{\sqrt{2}}\Phi_0(R)\varphi_{q_1}(r)(|\uparrow\downarrow\rangle_y - |\downarrow\uparrow\rangle_y). \quad (17)$$

The coefficients C_1^b-C_3^b are obtained by diagonalizing the effective low-energy Hamiltonian H_{eff}. Using ψ_{gr}^b to calculate the expectation values of $S_x(x)$ and $S_z(x)$, we find

$$\langle S_x^b(x)\rangle = \frac{\hbar}{2}C_x^b n_x^b(x) \quad (18)$$

and

$$\langle S_z^b(x)\rangle = \frac{\hbar}{2}C_z^b n_z^b(x), \quad (19)$$

where

$$C_x^b = C_1^b(C_2^b)^* + (C_1^b)^* C_2^b, \quad (20)$$

$$n_x^b(x) = \int_{-\infty}^{\infty} \Phi_0^2(R)\varphi_{q_0}^2(r)[\delta(x-x_1)+\delta(x-x_2)]d\vec{x}, \quad (21)$$

$$C_z^b = i[C_1^b(C_3^b)^* - (C_1^b)^* C_3^b], \quad (22)$$

and

$$n_z^b(x) = \int_{-\infty}^{\infty} \Phi_0^2(R)\varphi_{q_0}(r)\varphi_{q_1}(r)[\delta(x-x_1)-\delta(x-x_2)]d\vec{x}. \quad (23)$$

For two identical fermions, the ground state of the effective Hamiltonian is

$$\psi_{gr}^f = \frac{C_1^f}{\sqrt{2}}\Phi_0(R)\varphi_{q_1}(r)(|\uparrow\uparrow\rangle_y + |\downarrow\downarrow\rangle_y)$$

$$+\frac{C_2^f}{\sqrt{2}}\Phi_0(R)\varphi_{q_1}(r)(|\uparrow\downarrow\rangle_y + |\downarrow\uparrow\rangle_y)$$

$$+\frac{C_3^f}{\sqrt{2}}\Phi_0(R)\varphi_{q_0}(r)(|\uparrow\downarrow\rangle_y - |\downarrow\uparrow\rangle_y). \quad (24)$$

It can be seen that the structure of ψ_{gr}^f is very similar to that of ψ_{gr}^b, Eq. (17). The only differences are that the superscript b is replaced by f, that φ_{q_0} is replaced by φ_{q_1} (twice) and that φ_{q_1} is replaced by φ_{q_0} (once). It follows that the expressions that describe the spin structure of the fermionic system are nearly identical to those that describe the spin structure of the bosonic system. Specifically, Eqs. (18)-(23) apply to the fermionic system if the superscript b is replaced by f, φ_{q_0} is replaced by φ_{q_1}, and φ_{q_1} is replaced by φ_{q_0}.

We refer to $C_x^{b/f}$ and $C_z^{b/f}$ as the spin structure coefficients and to $n_x^{b/f}(x)$ and $n_z^{b/f}(x)$ as the spin structure densities. Note that these densities can be negative; a negative density indicates that the spin points in the negative direction. Importantly, the spin structure densities depend on g but are independent of k_{so} and Ω. The spin structure coefficients, in contrast, depend on k_{so}, Ω and g. To obtain the spin structure within the effective low-energy Hamiltonian approach, the spin structure density (see Fig. 3) gets multiplied by the spin structure coefficients, shown in Fig. 2 as a function of k_{so} for various g and fixed Ω ($\Omega = \hbar\omega/2$).

In general, the spin structures of the bosonic and fermionic systems differ. For a weak two-body interaction (small positive g) and Raman coupling strength $\Omega = \hbar\omega/2$ with vanishing spin-orbit coupling strength, the coupling between the singlet and the triplet states vanishes. Since the relative even parity state has a
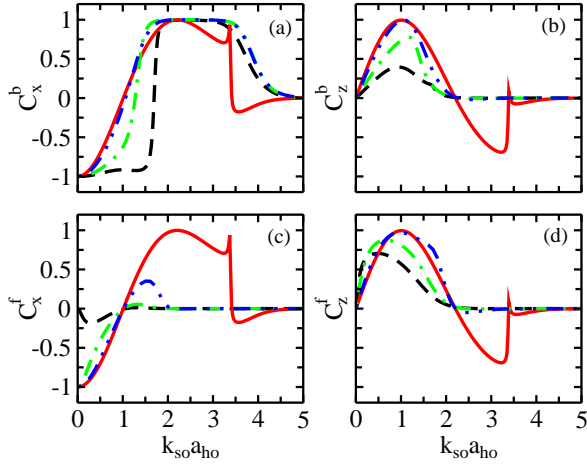
FIG. 2: (Color online) Spin structure coefficients (a) C_x^b, (b) C_z^b, (c) C_x^f, and (d) C_z^f for the $N = 2$ ground state obtained within the effective Hamiltonian approach for $\Omega = \hbar\omega/2$. The spin structure coefficients in (a) and (b) are for the system consisting of two identical bosons. The spin structure coefficients in (c) and (d) are for the system consisting of two identical fermions. Dashed, dot-dashed, dot-dot-dashed, and solid lines show the spin structure coefficients for $g = \sqrt{2}\hbar\omega a_{ho}, 3\sqrt{2}\hbar\omega a_{ho}, 15\sqrt{2}\hbar\omega a_{ho}$ and ∞, respectively. For infinitely large g (solid lines), the spin structure coefficients display a "sharp spike" at $k_{so}a_{ho} \approx 3.4$; this is the result of an avoided crossing between the ground and first
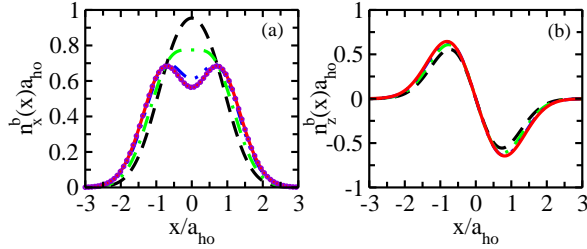

FIG. 3: (Color online) Spin structure densities for the $N = 2$ ground state for $\Omega = \hbar\omega/2$ and varying g. Panels (a) and (b) show the spin structure densities $n_x^b(x)$ and $n_z^b(x)$, respectively. Dashed, dot-dashed, dot-dot-dashed, and solid lines show the spin densities for $g = \sqrt{2}\hbar\omega a_{ho}, 3\sqrt{2}\hbar\omega a_{ho}, 15\sqrt{2}\hbar\omega a_{ho}$, and ∞, respectively. The spin structure density is independent of k_{so}. The spin structure density $n_x^f(x)$ is independent of g and shown by the circles in (a). The spin structure density $n_z^f(x)$ coincides with $n_z^b(x)$ for all g.

lower energy than the lowest relative odd-parity state for $g < \infty$, the ground states for two identical bosons and fermions are triplet and singlet states, respectively. Correspondingly, the coefficient C_3^b in Eq. (17) and the coefficients C_1^f and C_2^f in Eq. (24) vanish, yielding $\langle S_z^b(x) \rangle = \langle S_x^f(x) \rangle = \langle S_z^f(x) \rangle = 0$ and $\langle S_x^b(x) \rangle \neq 0$. For a non-vanishing spin-orbit coupling strength, the singlet and triplet states are coupled, leading to non-zero $\langle S_z^b(x) \rangle, \langle S_x^f(x) \rangle$, and $\langle S_z^f(x) \rangle$. With increasing g, the
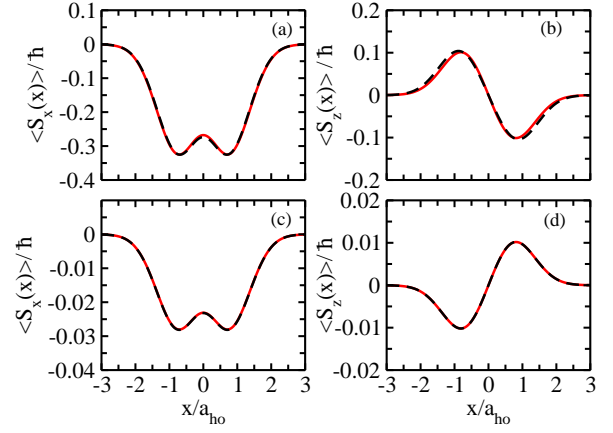

FIG. 4: (Color online) Benchmarking the effective Hamiltonian approach for the $N = 2$ ground state for $\Omega = \hbar\omega/2$ and $g = \infty$. Panels (a) and (b) show $\langle S_x(x) \rangle$ and $\langle S_z(x) \rangle$ for $k_{so}a_{ho} = 1/5$; panels (c) and (d) show $\langle S_x(x) \rangle$ and $\langle S_z(x) \rangle$ for $k_{so}a_{ho} = 4$. The solid lines show the spin structure obtained from the exact diagonalization while the dashed lines show the spin structure obtained within the effective Hamiltonian approach. On the scale shown, the solid and dashed lines nearly coincide.

energy difference between the singlet and triplet states for $k_{so} = 0$ decreases. As a consequence, for a fixed and relatively small k_{so}, the spin structures for two identical bosons and two identical fermions are more similar for larger g than for smaller g [see Figs. 2(a) and 2(c) for $k_{so}a_{ho} \lesssim 1.5$]. However, the coupling between the singlet and triplet states is weakened with increasing k_{so}. Specifically, for fixed g, the spin structures for bosons and fermions differ more as k_{so} increases [see Figs. 2(a) and 2(c) for $k_{so}a_{ho} > 2$]. For a larger k_{so}, a larger g is needed to get the triplet (singlet) state mixed significantly into the ground state for two identical fermions (bosons), resulting in similar spin structures for bosons and fermions. For an infinitely large g, the relative even and odd parity states have the same energy and the spin structures for bosonic and fermionic systems are identical for all k_{so} and Ω (see the solid lines in Fig. 2). This effect can be attributed to the Bose-Fermi duality (see next section for more details).

Our discussion so far has been based on the effective Hamiltonian approach. To benchmark this approach, we compare the effective Hamiltonian results with those obtained from the exact diagonalization for various g, k_{so}, and Ω combinations. The agreement is good for all cases considered. As an example, Fig. 4 compares the two-particle spin structure for infinite g and $\Omega = \hbar\omega/2$. Figures 4(a) and 4(b) are for small k_{so} ($k_{so}a_{ho} \ll 1$) and Figs. 4(c) and 4(d) are for large k_{so} ($k_{so}a_{ho} \gg 1$). The agreement between the effective Hamiltonian approach results (solid lines) and the exact diagonalization approach results (dashed lines) is very convincing.

IV. N-PARTICLE SYSTEM WITH $g = \infty$

A. Formulation

When the two-body coupling constant g is infinitely large, the particles cannot pass through each other. In the absence of the spin-orbit and Raman coupling terms, the atomic gas behaves like a Tonks-Girardeau gas [30, 63]. The Tonks-Girardeau gas has a large degeneracy and bosons fermionize [31, 63, 64]. The fact that the particles cannot pass through each other implies that the particles can be ordered. Since there are $N!$ ways to order the particles, the degeneracy of each eigenstate of H_{sr} with $g = \infty$ is $N!$ if the particle exchange symmetry is not being enforced. We thus pursue an approach where we first determine the eigenstates of $H_{sr}\hat{I}$ for a fixed particle ordering. The resulting eigenstates are then used either to calculate the eigenstates and eigenenergies of H through exact diagonalization or to calculate the eigenstates and eigenenergies of H_{eff} by identifying an appropriate subspace H_L. The fact that the particles can be ordered also allows us to derive an effective spin Hamiltonian H_{eff}^{spin} that is independent of the spatial coordinates.

For infinite g, the eigenstates of H_{sr} can be written as [31]

$$\phi_{n_1, n_2, \ldots, n_N}(\vec{x}) = D(n_1, n_2, \cdots, n_N)\Theta_{x_{j_1} < x_{j_2} < \cdots < x_{j_N}}, \tag{25}$$

where $D(n_1, n_2, \cdot\cdot\cdot, n_N)$ denotes the Slater determinant constructed from N one-dimensional harmonic oscillator eigenfunctions with quantum numbers $n_1, n_2, \cdot\cdot\cdot, n_N$ ($n_1 \neq n_2 \neq \cdots \neq n_N$). The sector function $\Theta_{x_{j_1} < x_{j_2} < \cdots < x_{j_N}}$ is 1 for $x_{j_1} < x_{j_2} < \cdots < x_{j_N}$ and zero otherwise. For the ground state, e.g., we have $n_1 = 0, n_2 = 1, \cdots, n_N = N - 1$. To construct eigenstates of $H_{sr}\hat{I}$, we include—as before—the spin part $|s_1, s_2, \cdots, s_N\rangle_y$. It is important to realize that there is no coupling between the eigenstates for different particle orderings, i.e., the Raman coupling term $(\Omega/2)V_R$ does not couple states with different particle orderings. This implies that the Hilbert space can be divided into $N!$ independent subspaces. A state in a given subspace can be mapped onto a state in a different subspace with the same eigenenergy through the application of one or more permutation operators. For example, for the $N = 3$ system, the particle ordering $x_1 < x_2 < x_3$ can be changed to the ordering $x_2 < x_1 < x_3$ through the application of the P_{12} operator. This property is used, after solving the problem in one of the $N!$ subspaces, to construct fully symmetric bosonic or fully anti-symmetric fermionic eigenstates from the non-symmetrized eigenstates that span one of the $N!$ distinct Hilbert spaces.

Without loss of generality, we discuss the ordering $x_1 < x_2 < \cdots < x_N$. Within this subspace, the evaluation of the Hamiltonian matrix elements involve integrals of the form

$$\mathcal{D}^j_{\substack{n_1, n_2 \ldots n_N \\ n'_1, n'_2, \cdots, n'_N}} = \int_{-\infty}^{\infty} D(n'_1, n'_2, \cdots, n'_N) \times$$

$$D(n_1, n_2, \cdots, n_N)\Theta_{x_1 < x_2 \cdots < x_N} e^{2ik_{so}x_j} d\vec{x}. \tag{26}$$

The evaluation of this integral for any N is detailed in Appendix A. Once the Hamiltonian matrix has been diagonalized, we determine the fully symmetric/anti-symmetric eigenstates by applying the N-particle symmetrizer/anti-symmetrizer.

Since we consider a fixed particle ordering, we define the sector Hamiltonian $H_{x_{j_1} < x_{j_2} < \cdots < x_{j_N}}$,

$$H_{x_{j_1} < x_{j_2} < \cdots < x_{j_N}} = H\Theta_{x_{j_1} < x_{j_2} < \cdots < x_{j_N}}, \tag{27}$$

which is non-zero only for the particle ordering $x_{j_1} < x_{j_2} < \cdots < x_{j_N}$. From the definitions of $H_{x_{j_1} < x_{j_2} < \cdots < x_{j_N}}$ and Y, it follows that $YH_{x_{j_1} < x_{j_2} < \cdots < x_{j_N}} = H_{x_{j_N} < x_{j_{N-1}} < \cdots < x_{j_1}}Y$, i.e., the Y operator does not commute with the sector Hamiltonian. We can, however, define a sector operator $Y_{x_{j_1} < x_{j_2} < \cdots < x_{j_N}}$ for the particle ordering $x_{j_1} < x_{j_2} < \cdots < x_{j_N}$, which commutes with the sector Hamiltonian with the same particle ordering. The eigenstates of the Y operator are then obtained by symmetrizing or anti-symmetrizing the eigenstates of the $Y_{x_{j_1} < x_{j_2} < \cdots < x_{j_N}}$ operator. The key idea is that the particle ordering after a change of the spatial and spin coordinates can be "restored" by exchanging the coordinates of the particles. Specifically, $Y_{x_{j_1} < x_{j_2} < \cdots < x_{j_N}}$ is defined through

$$Y_{x_{j_1} < x_{j_2} < \cdots < x_{j_N}} = (\pm 1)^{[\frac{N}{2}]}$$
$$P_{j_1 j_N} P_{j_2 j_{N-1}} \cdots P_{j_{[\frac{N}{2}]} j_{N+1-[\frac{N}{2}]}} Y, \tag{28}$$

where $[N/2]$ denotes the integer part of $N/2$, and the plus and minus signs apply to identical bosons and fermions, respectively. It can be proven readily that $Y_{x_{j_1} < x_{j_2} < \cdots < x_{j_N}}$ commutes with $H_{x_{j_1} < x_{j_2} < \cdots < x_{j_N}}$. To show that the eigenstates of the Y operator are obtained by symmetrizing or anti-symmetrizing the eigenstates of $Y_{x_{j_1} < x_{j_2} < \cdots < x_{j_N}}$, let $\psi_{x_{j_1} < x_{j_2} < \cdots < x_{j_N}}$ denote a wave function in the subspace with the ordering $x_{j_1} < x_{j_2} < \cdots < x_{j_N}$ with the property

$$Y_{x_{j_1} < x_{j_2} < \cdots < x_{j_N}} \psi_{x_{j_1} < x_{j_2} < \cdots < x_{j_N}}$$
$$= b\psi_{x_{j_1} < x_{j_2} < \cdots < x_{j_N}}. \tag{29}$$

Taking advantage of

$$S^s P_{j_1 j_N} P_{j_2 j_{N-1}} \cdots P_{j_{[\frac{N}{2}]} j_{N+1-[\frac{N}{2}]}} = S^s, \tag{30}$$

$$S^a (-1)^{[\frac{N}{2}]} P_{j_1 j_N} P_{j_2 j_{N-1}} \cdots P_{j_{[\frac{N}{2}]} j_{N+1-[\frac{N}{2}]}} = S^a, \tag{31}$$

and the fact that Y commutes with $S^{s(a)}$, where $S^{s(a)}$ denotes the N-particle symmetrizer (anti-symmetrizer),

we obtain

$$S^{s(a)} Y_{x_{j_1} < x_{j_2} < \cdots < x_{j_N}} \psi_{x_{j_1} < x_{j_2} < \cdots < x_{j_N}} =$$
$$Y S^{s(a)} \psi_{x_{j_1} < x_{j_2} < \cdots < x_{j_N}}. \qquad (32)$$

Using Eq. (29), Eq. (32) leads to $Y S^{s(a)} \psi_{x_{j_1} < x_{j_2} < \cdots < x_{j_N}} = b S^{s(a)} \psi_{x_{j_1} < x_{j_2} < \cdots < x_{j_N}}$, i.e., $S^{s(a)} \psi_{x_{j_1} < x_{j_2} < \cdots < x_{j_N}}$ is an eigenstate of Y with eigenvalue b.

To construct the Hamiltonian H_{eff}, we proceed similarly, i.e., we also work with a particular particle ordering. The space H_L is spanned by the states $D(0, 1, \cdots, N-1)\Theta_{x_1 < x_2 < \cdots < x_N} |s_1, s_2, \cdots, s_N\rangle_y$, where the spin function can take 2^N different arrangements. Correspondingly, the space H_H is spanned by all other unperturbed eigenstates with the ordering $x_1 < x_2 < \cdots < x_N$. The Hamiltonian matrix for H_{eff} is constructed and diagonalized, and states with good symmetry are obtained following the same steps as discussed above.

We now discuss the construction of an effective spin Hamiltonian. Since the particles can be ordered in $N!$ distinct ways, the ground state is $N!$-fold degenerate. We integrate out the spatial degrees of freedom of the effective Hamiltonian H_{eff}, yielding a spin Hamiltonian H_{eff}^{spin} that depends only on the spin degrees of freedom. Specifically, since the Hilbert space H_L contains exactly one spatial wavefunction with ordering $x_1 < x_2 < \cdots < x_N$, we define H_{eff}^{spin} through $H_{eff}^{spin} = \int_{-\infty}^{\infty} D^*(0, 1, \cdots, N-1) H_{eff} D(0, 1, \cdots, N-1)\Theta_{x_1 < x_2 < \cdots < x_N} d\vec{x}$. Using that the spins are also ordered, H_{eff}^{spin} can be compactly written as

$$H_{eff}^{spin} = \left(E_0 - \frac{N \hbar^2 k_{so}^2}{2m} \right) \hat{I} + \frac{\Omega}{2} \sum_{j=1}^{N} \vec{B}_j \cdot \vec{\sigma}_j$$
$$+ \frac{\Omega^2}{2\hbar\omega} \sum_{j<k} \vec{\sigma}_j^T M_{jk} \vec{\sigma}_k + \frac{\Omega^2}{4\hbar\omega} \sum_j (a_{jj} + b_{jj}), \qquad (33)$$

where

$$\vec{\sigma}_j^T = (\sigma_x^{(j)}, \sigma_z^{(j)}) \qquad (34)$$

and

$$\vec{B}_j^T = (B_x^{(j)}, B_z^{(j)}). \qquad (35)$$

E_0 is the ground state energy of H_{sr}, $E_0 = \hbar\omega N^2/2$, and M_{jk} is a 2×2 matrix (see below). The first, second, and third terms on the right hand side of Eq. (33) come from $H_{eff}^{(0)}$, $H_{eff}^{(1)}$, and $H_{eff}^{(2)}$, respectively. The fourth term on the right hand side of Eq. (33) also comes from $H_{eff}^{(2)}$; it accounts for the (spin-independent) onsite interaction, with a_{jj} and b_{jj} defined below in Eqs. (39) and (40). We find

$$B_x^{(j)} = Re(\mathcal{D}^j_{\substack{0,1,2,\cdots,N-1 \\ 0,1,2,\cdots,N-1}}) \qquad (36)$$

and

$$B_z^{(j)} = Im(\mathcal{D}^j_{\substack{0,1,2,\cdots,N-1 \\ 0,1,2,\cdots,N-1}}). \qquad (37)$$

The matrix M_{jk} can be written as

$$M_{jk} = \begin{bmatrix} a_{jk} & -c_{jk} \\ c_{kj} & b_{jk} \end{bmatrix}, \qquad (38)$$

where

$$\frac{a_{jk}}{\hbar\omega} = \sum_{\substack{(n_1, n_2, n_3, \cdots, n_N) \\ \neq (0,1,2,\cdots,N-1)}} \frac{Re(\mathcal{D}^j_{\substack{0,1,2,\cdots,N-1 \\ n_1,n_2,\cdots,n_N}}) Re(\mathcal{D}^k_{\substack{0,1,2,\cdots,N-1 \\ n_1,n_2,\cdots,n_N}})}{E_0 - E_{n_1, n_2, \cdots, n_N}},$$
$$\qquad (39)$$

$$\frac{b_{jk}}{\hbar\omega} = \sum_{\substack{(n_1, n_2, n_3, \cdots, n_N) \\ \neq (0,1,2,\cdots,N-1)}} \frac{Im(\mathcal{D}^j_{\substack{0,1,2,\cdots,N-1 \\ n_1,n_2,\cdots,n_N}}) Im(\mathcal{D}^k_{\substack{0,1,2,\cdots,N-1 \\ n_1,n_2,\cdots,n_N}})}{E_0 - E_{n_1, n_2, \cdots, n_N}},$$
$$\qquad (40)$$

$$\frac{-c_{jk}}{\hbar\omega} = \sum_{\substack{(n_1, n_2, n_3, \cdots, n_N) \\ \neq (0,1,2,\cdots,N-1)}} \frac{Re(\mathcal{D}^j_{\substack{0,1,2,\cdots,N-1 \\ n_1,n_2,\cdots,n_N}}) Im(\mathcal{D}^k_{\substack{0,1,2,\cdots,N-1 \\ n_1,n_2,\cdots,n_N}})}{E_0 - E_{n_1, n_2, \cdots, n_N}},$$
$$\qquad (41)$$

and

$$\frac{c_{kj}}{\hbar\omega} = \sum_{\substack{(n_1, n_2, n_3, \cdots, n_N) \\ \neq (0,1,2,\cdots,N-1)}} \frac{Im(\mathcal{D}^j_{\substack{0,1,2,\cdots,N-1 \\ n_1,n_2,\cdots,n_N}}) Re(\mathcal{D}^k_{\substack{0,1,2,\cdots,N-1 \\ n_1,n_2,\cdots,n_N}})}{E_0 - E_{n_1, n_2, \cdots, n_N}}.$$
$$\qquad (42)$$

The second and third terms on the right hand side of Eq. (33) correspond to a single spin term (this is the first-order term) and a spin-spin term, respectively. For small k_{so}, the first-order term dominates. The spin at each slot j follows the effective magnetic $\vec{B}_j$ field and the system has a rotational spin structure [21]. In this regime, the spin correlations are very weak. The eigenstates of H_{eff}^{spin} include equal weights of each spin state, namely, $P_{|M_s|}$ is proportional to the number of spin states that have the same absolute value of M_s (see Table I). For example, for $N = 3$, two states have $|M_s| = 0$ and six states have $|M_s| = 1$, which yields that $P_{|M_s|=0} = 1/4$ and $P_{|M_s|=1} = 3/4$.

For fairly large k_{so}, the second-order term dominates over the first-order term, i.e., the spin correlations are very strong and the spin structure is non-trivial (see also discussion around Fig. 1). For large k_{so}, we find numerically that the nearest neighbor spin-spin interactions dominate. For example, $|a_{12}|$ is much larger than $|a_{13}|$. It should be noted, though, that the summands entering into a_{12} and a_{13} are of roughly the same order of magnitude. Moreover, we find that the nearest-neighbor coefficients $a_{(jk)}, b_{(jk)}, c_{(jk)}$ and $c_{(kj)}$ are, for fixed k_{so}, approximately equal; here, the subscript (jk) indicates

that j and k are related via $j = k - 1$. We have checked this for $N \leq 4$. For large N, we cannot rule out that the values of the coefficients depend on the slot, possibly yielding more complicated spin structures than discussed in this work. For $a_{(jk)} = b_{(jk)} = c_{(jk)} = c_{(kj)}$, the matrix M_{jk} simplifies dramatically,

$$M_{(jk)} = A \begin{bmatrix} 1 & -1 \\ 1 & 1 \end{bmatrix} \tag{43}$$

for $j = k - 1$ and $M_{jk} \approx 0$ for $j \neq k - 1$. In Eq. (43), A is a negative dimensionless constant. In this case, the last term on the right hand side of Eq. (33) reduces to

$$\frac{\Omega^2}{2\hbar\omega} \sum_{j<k} \vec{\sigma}_j^T M_{jk} \vec{\sigma}_k = \frac{\Omega^2}{2\hbar\omega} \times$$
$$A \sum_{(jk)} \left[\vec{\sigma}_j \cdot \vec{\sigma}_k - (\sigma_x^{(j)}\sigma_z^{(k)} - \sigma_z^{(j)}\sigma_x^{(k)}) \right]. \tag{44}$$

The first term in square brackets on the right hand side of Eq. (44) corresponds to the usual Heisenberg exchange term. The term in round brackets on the right hand side of Eq. (44) is readily indentified as the y-component of the cross product between two three-dimensional spin vectors. This term is the one-dimensional analog of the anisotropic Dzyaloshinskii-Moriya exchange term [60–62].

To obtain the spin structure of this approximate effective spin Hamiltonian, we rewrite Eq. (44) as

$$\frac{\Omega^2}{2\hbar\omega} \sum_{j<k} \vec{\sigma}_j^T M_{jk} \vec{\sigma}_k = \frac{\Omega^2}{2\hbar\omega} \times$$
$$A \sum_{(jk)} [2(1-i)\sigma_-^{(j)}\sigma_+^{(k)} + 2(1+i)\sigma_+^{(j)}\sigma_-^{(k)}], \tag{45}$$

where $\sigma_\pm^{(j)} = (\sigma_x^{(j)} \mp i\sigma_z^{(j)})/2$. If we neglect the first-order term and use the right hand side of Eq. (45) in Eq. (33), we find that H_{eff}^{spin} commutes with σ_y. Moreover, this approximate Hamiltonian H_{eff}^{spin} also has time reversal symmetry, i.e., it commutes with $i\sigma_y K$, where K changes the quantity that it acts on into the complex conjugate of that quantity. However, $i\sigma_y K$ and σ_y do not commute. Using additionally the property that $K|s\rangle_y = |\bar{s}\rangle_y$, one can show that the eigenstates with M_s and $-M_s$ of the approximate effective spin Hamiltonian have the same energy provided $|M_s| > 0$, i.e., the states with $|M_s| > 0$ are two-fold degenerate. The first-order term breaks the degeneracy of the eigenstates with M_s and $-M_s$. As a result, the eigenstates of the full Hamiltonian H_{eff}^{spin} (including zero-, first-, and second-order terms) are, for $k_{so} \to \infty$, approximately superpositions of states that have the same absolute value of the M_s quantum number. The $\sigma_-^{(j)}\sigma_+^{(k)}$ and $\sigma_+^{(j)}\sigma_-^{(k)}$ terms correspond to nearest neighbor spin hopping. These terms lead to a lowering of the energy. The more possibility for the nearest neighbor spin hopping a state has, the

N	$k_{so} \to 0$	$k_{so} \to \infty$
2	$P_0 = 1/2, P_2 = 1/2$	$P_0 = 1, P_2 = 0$
3	$P_1 = 3/4, P_3 = 1/4$	$P_1 = 1, P_3 = 0$
4	$P_0 = 3/8, P_2 = 1/2, P_4 = 1/8$	$P_0 = 1, P_2 = 0, P_4 = 0$

TABLE I: Spin correlations for the ground state in the limiting cases $k_{so} \to 0$ and $k_{so} \to \infty$ for various N. The probability $P_{|M_s|}$ that the ground state has the absolute value of M_s is reported. For small k_{so}, all spin states are equally weighted, which means that $P_{|M_s|}$ is proportional to the number of spin states that have the same $|M_s|$. For large k_{so}, the spin states are not equally weighted. In this case, the ground state contains only spin states with the minimum allowed $|M_s|$.

lower the energy associated with that state is. For example, the states $|\uparrow\downarrow\rangle_y$ and $|\downarrow\uparrow\rangle_y$ are "connected" via nearest neighbor hoppings while the states $|\uparrow\uparrow\rangle_y$ and $|\downarrow\downarrow\rangle_y$ are not connected with each other or with $|\uparrow\downarrow\rangle_y$ or $|\downarrow\uparrow\rangle_y$ via nearest neighbor hopping. Correspondingly, the $N = 2$ ground state is a linear combination of the $|\uparrow\downarrow\rangle_y$ and $|\downarrow\uparrow\rangle_y$ states. For $N = 3$, e.g., the state $|\uparrow\uparrow\downarrow\rangle_y$ is connected to $|\uparrow\downarrow\uparrow\rangle_y$ via $\sigma_2^{(-)}\sigma_3^{(+)}$ and to $|\downarrow\uparrow\uparrow\rangle_y$ via $\sigma_1^{(-)}\sigma_3^{(+)}$ while the state $|\downarrow\downarrow\uparrow\rangle_y$ is connected to $|\downarrow\uparrow\downarrow\rangle_y$ via $\sigma_2^{(+)}\sigma_3^{(-)}$ and to $|\uparrow\downarrow\downarrow\rangle_y$ via $\sigma_1^{(+)}\sigma_3^{(-)}$. Correspondingly, the $N = 3$ ground state is a linear combination of all $|M_s| = 1$ states. Table I shows the values of $P_{|M_s|=m}$ in the limits $k_{so} \to 0$ and $k_{so} \to \infty$ for $N = 2 - 4$.

Figure 5 shows the probability to find the system in a state with a given $|M_s|$ as a function of k_{so} for the two-, three-, and four-particle systems with infinitely large g (see the next subsection for the calculational details). For large k_{so}, $P_{|M_s|=0} = 1$ for the two-particle system, $P_{|M_s|=1} = 1$ for the three-particle system, and $P_{|M_s|=0} = 1$ for the four-particle system.

B. Application to systems with $N = 2 - 4$

This section evaluates the expectation values of the spin operators defined in Eqs. (7)-(9) for the three- and four-particle systems with infinite g. For $N = 2$, the expectation values of $S_x(x)$ and $S_z(x)$ for infinitely large g have been calculated in Sec. III. For $N = 3$, the non-symmetrized ground state wave function of the effective Hamiltonian H_{eff} is

$$\psi_{gr} = \frac{D(0,1,2)}{\sqrt{2}} \Theta_{x_1<x_2<x_3} \times$$
$$\left[C_1(|\uparrow\uparrow\uparrow\rangle_y - |\downarrow\downarrow\downarrow\rangle_y) + C_2(|\uparrow\uparrow\downarrow\rangle_y - |\uparrow\downarrow\downarrow\rangle_y) \right.$$
$$\left. + C_3(|\uparrow\downarrow\uparrow\rangle_y - |\downarrow\uparrow\downarrow\rangle_y) + C_4(|\downarrow\uparrow\uparrow\rangle_y - |\downarrow\downarrow\uparrow\rangle_y) \right]. \tag{46}$$

The coefficients C_1-C_4 are obtained by diagonalizing the effective low-energy Hamiltonian H_{eff}. Using this wave function, the expectation values of $S_x(x)$ and $S_z(x)$ for
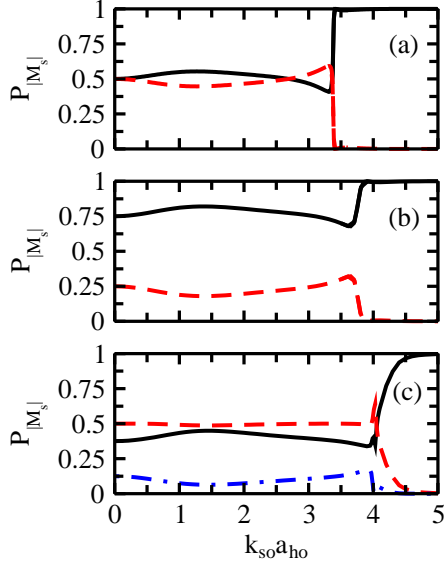
FIG. 5: (Color online) Expectation value of $P_{|M_s|=m}$ for (a) $N = 2$, (b) $N = 3$, and (c) $N = 4$ with $g = \infty$ and $\Omega = \hbar\omega/2$ as a function of k_{so}. (a) The solid and dashed lines show $P_{|M_s|=0}$ and $P_{|M_s|=2}$, respectively. (b) The solid and dashed lines show $P_{|M_s|=1}$ and $P_{|M_s|=3}$, respectively. (c) The solid, dashed, and dot-dashed lines show $P_{|M_s|=0}$, $P_{|M_s|=2}$ and $P_{|M_s|=4}$, respectively.

the three-particle system are

$$\langle S_x(x)\rangle = \frac{\hbar}{2}[C_{1x}n_{1x}(x) + C_{2x}n_{2x}(x)] \quad (47)$$

and

$$\langle S_z(x)\rangle = \frac{\hbar}{2}C_z n_z(x). \quad (48)$$

The coefficients C_{1x}, C_{2x}, and C_z, which depend on the coefficients $C_1 - C_4$ in Eq. (46), and the expressions for the density functions $n_{1x}(x)$, $n_{2x}(x)$, and $n_z(x)$ are given in Appendix B. Figure 6 shows the spin coefficients and spin densities for $N = 3$ with infinite g for different k_{so}. For fixed x, $\langle S_x(x)\rangle$ and $\langle S_z(x)\rangle$ oscillate with k_{so} for $k_{so} \leq k_{so}^{cr}$, where $a_{ho}k_{so}^{cr} \approx 3.7$. The oscillations disappear for k_{so} greater than k_{so}^{cr}.

For $N = 4$, the non-symmetrized ground state wave function of the effective Hamiltonian H_{eff} is

$$\psi_{gr} = D(0,1,2,3)\Bigg\{\frac{1}{\sqrt{2}}\Big[C_1\left(|\uparrow\uparrow\uparrow\uparrow\rangle_y + |\downarrow\downarrow\downarrow\downarrow\rangle_y\right)$$

$$+C_2\left(|\uparrow\uparrow\uparrow\downarrow\rangle_y + |\uparrow\downarrow\downarrow\downarrow\rangle_y\right) + C_3\left(|\uparrow\uparrow\downarrow\uparrow\rangle_y + |\downarrow\uparrow\downarrow\downarrow\rangle_y\right)$$

$$+C_4\left(|\uparrow\downarrow\uparrow\uparrow\rangle_y + |\downarrow\downarrow\uparrow\downarrow\rangle_y\right) + C_5\left(|\downarrow\uparrow\uparrow\uparrow\rangle_y + |\downarrow\downarrow\downarrow\uparrow\rangle_y\right)$$

$$+C_8\left(|\uparrow\downarrow\downarrow\uparrow\rangle_y + |\downarrow\uparrow\uparrow\downarrow\rangle_y\right)\Big] + C_6|\uparrow\uparrow\downarrow\downarrow\rangle_y + C_7|\uparrow\downarrow\uparrow\downarrow\rangle_y$$

$$+C_9|\downarrow\downarrow\uparrow\uparrow\rangle_y + C_{10}|\downarrow\uparrow\downarrow\uparrow\rangle_y\Bigg\}\Theta_{x_1<x_2<x_3<x_4} \quad (49)$$

The coefficients C_1-C_{10} are obtained by diagonalizing the effective low-energy Hamiltonian H_{eff}. Using this wave
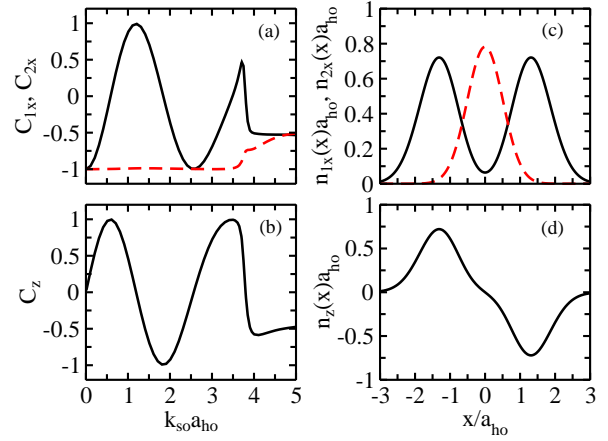

FIG. 6: (Color online) Spin structure for the three-particle system with $g = \infty$ and $\Omega = \hbar\omega/2$ as a function of k_{so}. (a) The solid and dashed lines show the spin structure coefficients C_{1x} and C_{2x}, respectively. (b) The solid and dashed lines show the spin structure coefficient C_z. (c) The solid and dashed lines show the spin structure densities $n_{1x}(x)$ and $n_{2x}(x)$, respectively. (d) The solid line shows the spin structure density $n_z(x)$.

function, the expectation values of $S_x(x)$ and $S_z(x)$ for the four-particle system are

$$\langle S_x(x)\rangle = \frac{\hbar}{2}[C_{1x}n_{1x}(x) + C_{2x}n_{2x}(x)] \quad (50)$$

and

$$\langle S_z(x)\rangle = \frac{\hbar}{2}[C_{1z}n_{1z}(x) + C_{2z}n_{2z}(x)]. \quad (51)$$

Expressions for the coefficients C_{1x}, C_{2x}, C_{1z}, and C_{2z} and the density functions $n_{1x}(x), n_{2x}(x), n_{1z}(x)$, and $n_{2z}(x)$ are given in Appendix B. Figures 7(a) and 7(b) show that the spin structure coefficients go to approximately zero at $a_{ho}k_{so}^{cr} \approx 4.3$.

To visualize the spin structure, Figs. 8-10 show the spin vector $(\langle S_x(x)\rangle, \langle S_z(x)\rangle)$ at each "slot" as a function of k_{so} for $N = 2 - 4$ with $g = \infty$. In each figure, the top to bottom panels correspond to the leftmost to the rightmost slot. For $k_{so} \lesssim k_{so}^{cr}$, the spin vector rotates with increasing k_{so}. For $k_{so} \gtrsim k_{so}^{cr}$, the spin-spin interaction term dominates. For $N = 2$ and $N = 4$, the magnitude of the spin vector at each slot is approximately zero for $k_{so} \gtrsim k_{so}^{cr}$. For $N = 3$, in contrast, the magnitude of the spin vector at each slot is fixed and the orientation of the spin vector is, to a good approximation, independent of k_{so}. Taking the ground state of the approximate effective Hamiltonian to calculate $\langle S_x(x)\rangle$ and $\langle S_z(x)\rangle$, we find $\langle S_x(x)\rangle \approx \langle S_z(x)\rangle \approx -\hbar/2$ for the leftmost slot and $\langle S_x(x)\rangle \approx -\langle S_z(x)\rangle \approx -\hbar/2$ for the rightmost slot for $k_{so} \gtrsim k_{so}^{cr}$. This behavior is a signature of the spin-spin correlations. For even N systems, the ground state in the large k_{so} limit is a superposition of spin states with $|M_s| = 0$. Two states $|s_1, s_2, \cdots, s_N\rangle_y$ and $|s_1', s_2', \cdots, s_N'\rangle_y$,
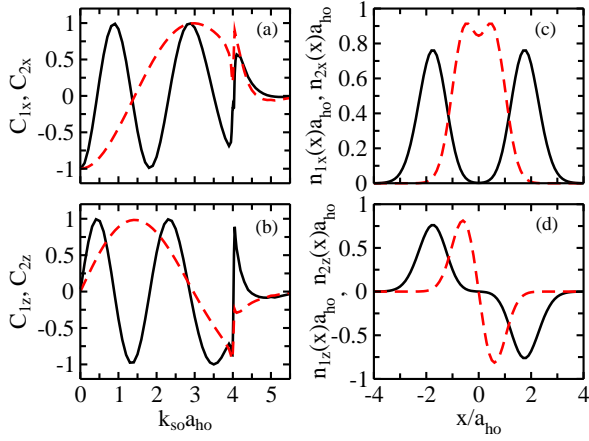
FIG. 7: (Color online) Spin structure for the four-particle system with $g = \infty$ and $\Omega = \hbar\omega/2$ as a function of k_{so}. (a) The solid and dashed lines show the spin structure coefficients C_{1x} and C_{2x}. (b) The solid and dashed lines show the spin structure coefficients C_{1z} and C_{2z}. (c) The solid and dashed lines show the spin structure densities $n_{1x}(x)$ and $n_{2x}(x)$. (d) The solid and dashed lines show the spin structure densities $n_{1z}(x)$ and $n_{2z}(x)$.
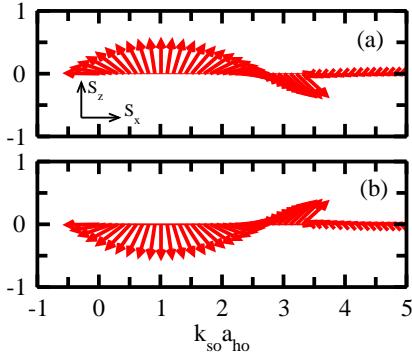

FIG. 8: (Color online) The spin structure for two identical particles with $g = \infty$ and $\Omega = \hbar\omega/2$. Panel (a) shows the spin vector at the leftmost slot while panel (b) shows the spin vector at the rightmost slot. For $k_{so} \lesssim k_{so}^{cr} \approx 3.4/a_{ho}$, the spin vector at each slot follows the local effective $\vec{B}$ field. The spin vector rotates with increasing k_{so}. For $k_{so} \gtrsim k_{so}^{cr}$, the spin-spin interaction is dominant, resulting in an approximately vanishing spin vector at each slot.

both with $M_s = 0$, contain an even number of s_j and s'_j for which $s_j \neq s'_j$. For $N = 2$, e.g., to get the state $|\uparrow\downarrow\rangle_y$ from the state $|\downarrow\uparrow\rangle_y$, two spin flips are needed. For odd N systems, the ground state in the large k_{so} limit is a superposition of spin states with $|M_s| = 1$. Two states $|s_1, s_2, \cdots, s_N\rangle_y$ and $|s'_1, s'_2, \cdots, s'_N\rangle_y$, both with $|M_s| = 1$, contain an odd number of s_j and s'_j for which $s_j \neq s'_j$. For $N = 3$, e.g., to get the state $|\uparrow\uparrow\downarrow\rangle_y$ from the state $|\uparrow\downarrow\downarrow\rangle_y$, one spin flip is needed. The non-vanishing $\langle S_x(x)\rangle$ and $\langle S_z(x)\rangle$ arise from a superposition of states that contain $N - 1$ identical spins ($s_j = s'_j$) and one pair
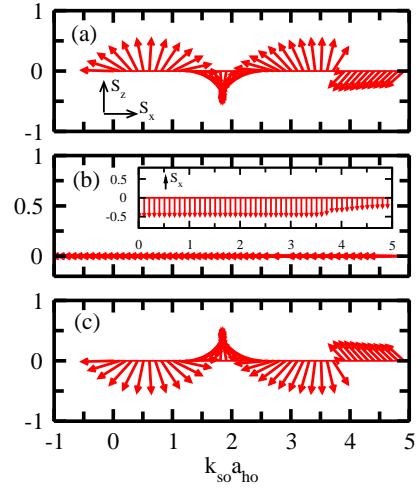

FIG. 9: (Color online) The spin structure for three identical particles with $g = \infty$ and $\Omega = \hbar\omega/2$. Panel (a) shows the spin vector at the leftmost slot, panel (b) shows the spin vector at the middle slot, and panel (c) shows the spin vector at the rightmost slot. For $k_{so} \lesssim k_{so}^{cr} \approx 3.7/a_{ho}$, the spin vector at each slot follows the local effective $\vec{B}$ field. The spin vector rotates with increasing k_{so}. For $k_{so} \gtrsim k_{so}^{cr}$, the spin-spin interaction is dominant, resulting in a spin vector with approximately constant magnitude and orientation at each slot. The inset in (b) replots the spin vector using a different orientation of the coordinate system.

of opposite spins ($s_j \neq s'_j$). As a result, the spin vector ($\langle S_x(x)\rangle, \langle S_z(x)\rangle$) vanishes for even N systems with large k_{so} while that for odd N systems is finite and approximately constant.

V. CONCLUSION

Spin Hamiltonian play an important role in understanding material properties such as the transition from ferromagnetic to anti-ferromagnetic order. Much effort has gone into identifying clean model systems with which to emulate spin dynamics. Notable examples include trapped ion systems, ranging from small two- or three-ion chains [65, 66] to large two-dimensional ion crystals [67, 68], and ultracold atoms [16, 17, 56–59, 69, 70]. This paper considered ultracold harmonically trapped one-dimensional atoms with infinitely large two-body contact interactions subject to spin-orbit and Raman couplings and derived an effective low-energy spin Hamiltonian that is accurate to second order in the Raman coupling strength Ω. It was shown explicitly for $N = 2 - 4$ particles that tuning the spin-orbit coupling strength from a regime where the spins independently follow the effective external magnetic field generated by the Raman coupling to a regime where the spin dynamics is governed by the nearest neighbor spin-spin interactions is feasible. While the examples presented are for small particle numbers, Appendix A derived a number of identities appli-
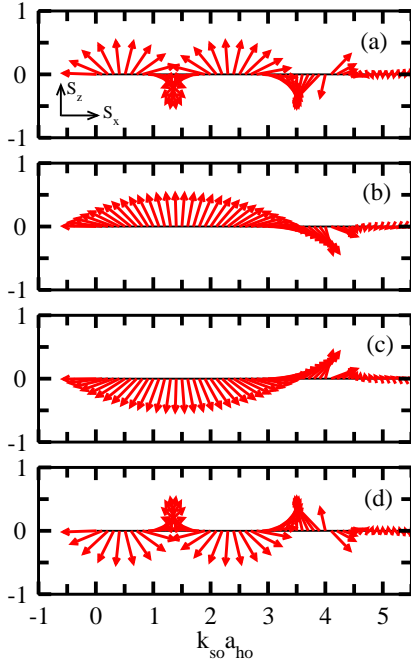
FIG. 10: (Color online) The spin structure for four identical particles with $g = \infty$ and $\Omega = \hbar\omega/2$. Panel (a) shows the spin vector at the leftmost slot. Panel (b) shows the spin vector at the second slot from the left. Panel (c) shows the spin vector at the third slot from the left. Panel (d) shows the spin vector at the rightmost slot. For $k_{so} \lesssim k_{so}^{cr} \approx 4.3/a_{ho}$, the spin vector at each slot follows the local effective $\vec{B}$ field. The spin vector rotates with increasing k_{so}. For $k_{so} \gtrsim k_{so}^{cr}$, the spin-spin interaction is dominant, resulting in an approximately vanishing spin vector at each slot.

cable to systems of arbitrary size that should facilitate extensions to larger N and that may find applications in calculating the momentum distribution or related observables for strongly-interacting one-dimensional atomic gases without spin-orbit coupling.

The relevance of the effective spin Hamiltonian derived in this paper is two-fold. (i) As already alluded to above, this paper introduced a new means to realize a tunable effective spin Hamiltonian. (ii) The spin Hamiltonian language provides a physically transparent means to understand the intricate dynamics of strongly correlated spin-orbit coupled ultracold atomic systems.

Throughout this paper, explicit calculations were performed for the Raman coupling strength $\Omega = \hbar\omega/2$. For this coupling strength, the energy difference for $k_{so} \geq k_{so}^{cr}$ between the ground state and the first excited state is of the order of $10^{-4}\hbar\omega$ for $N = 2 - 4$ particles. This small energy difference may make it challenging to experimen-tally occupy the ground state. Since the second-order term is proportional to $\Omega^2/(\hbar\omega)$, the critical k_{so}^{cr} decreases with increasing Ω. For $\Omega = 4\hbar\omega$ and $N = 3$, e.g., we find $k_{so}^{cr} a_{ho} \approx 3.5$ and an energy splitting between the ground state and the first excited state with the same symmetry of the order of $10^{-2}\hbar\omega$. This energy splitting appears much more tractable experimentally.

An important question is then whether the effective second-order low-energy spin Hamiltonian is applicable for such large Ω. To investigate this question, we compared the results obtained by solving the second-order effective Hamiltonian with the results obtained from the diagonalization of the full Hamiltonian. The agreement is very good for $k_{so} \geq k_{so}^{cr}$ (we excluded the regime $k_{so} \gg k_{so}^{cr}$), suggesting that the third-order term, which is proportional to $\Omega^3/(\hbar\omega)^2$, is suppressed. Naively, one expects the third-order term to be enhanced by $\Omega/(\hbar\omega)$ compared to the second-order term for $\Omega > \hbar\omega$, making a perturbative approach meaningless. However, the full perturbative expression also contains the matrix elements and energy denominator. It turns out that the product of three matrix elements is highly suppressed compared to the product of two matrix elements. We conclude that the second-order effective spin Hamiltonian capture the physics, including the spin structure up to, at first sight, surprisingly large $\Omega/(\hbar\omega)$ for relatively large k_{so}.

A key ingredient that went into deriving the effective low-energy spin Hamiltonian is that the particles in one-dimensional space can be ordered if the two-body coupling constant g is infinitely large. For finite g, this is not the case, i.e., particles are allowed to pass through each other. In this case, a low-energy Hamiltonian that depends on the spatial and spin degrees of freedom was derived (in fact, the effective spin Hamiltonian for $g = \infty$ was derived by taking this Hamiltonian and integrating out the spatial degrees of freedom). The low-energy Hamiltonian was tested for two particles and shown to reproduce the full Hamiltonian dynamics well. Moreover, it was shown to provide a powerful theoretical framework within which to interpret the full Hamiltonian results. We believe that the formalism can be applied to larger one-dimensional system and extended to higher-dimensional systems.

Appendix A: Calculation of involved integrals

This section contains the evaluation of the integral given in Eq. (26). We denote the nth harmonic oscillator eigenstate by $\varphi_n(x)$, $\varphi_n(x) = N_n H_n(x/a_{ho})e^{-x^2/(2a_{ho}^2)}$, where $N_n = 1/\sqrt{\sqrt{\pi}n!2^n a_{ho}}$ is the normalization constant

and $H_n(x)$ the nth Hermite polynomial. Throughout this appendix, we set $a_{ho} = 1$, i.e., we work with dimensionless spatial coordinates. Expanding the Slater determinant $D(n_1, n_2, \cdots, n_N)$, we have

$$D(n_1, n_2, \cdots, n_N) = \sum_{p_1, p_2, \cdots, p_N} (-1)^{P_{p_1, p_2, \cdots, p_N}} \Pi_{l=1}^N \varphi_{n_{p_l}}(x_l), \tag{A1}$$

where $p_1, p_2, \cdots, p_N$ denotes a permutation of $1, 2, \cdots, N$ and $P_{p_1, p_2, \cdots, p_N}$ the number of permutations needed to obtain the order $p_1, p_2, \cdots, p_N$ from the ordinary order $1, 2, \cdots, N$. The sum in Eq. (A1) contains $N!$ terms. Note that since the eigenstates $\phi_{n_1, n_2, \cdots, n_N}(\vec{x})$ in Eq. (25) are only non-zero for a particular particle ordering, we do not need a prefactor of $1/\sqrt{N!}$ in front of the Slater determinant to normalize the eigenstates. Equation (26) contains two different Slater determinants (D functions), one with arguments $n_1, \cdots, n_N$ and the other with arguments $n_1', \cdots, n_n'$. To simplify the notation, we use $m_1, \cdots, m_N$ instead of $n_1', \cdots, n_n'$ in what follows. The corresponding permutations are denoted by $q_1, \cdots, q_N$. With these conventions, Eq. (26) becomes

$$\mathcal{D}^j_{\substack{n_1, n_2, \cdots, n_N \\ m_1, m_2, \cdots, m_N}} = \int_{-\infty}^{\infty} \left(\sum_{p_1, p_2, \cdots, p_N} (-1)^{P_{p_1, p_2, \cdots, p_N}} \Pi_{l=1}^N \varphi_{n_{p_l}}(x_l) \right)$$
$$\left(\sum_{q_1, q_2, \cdots, q_N} (-1)^{P_{q_1, q_2, \cdots, q_N}} \Pi_{l=1}^N \varphi_{m_{q_l}}(x_l) \right) \Theta_{x_1 < x_2 < \cdots < x_N} e^{2ik_{so}x_j} d\vec{x}. \tag{A2}$$

Since the integral in Eq. (A2) can be interpreted as a Fourier transform with respect to the coordinate x_j, we first evaluate the integral over the coordinates $x_1, \cdots, x_{j-1}, x_{j+1}, \cdots, x_N$. Except for the sector function $\Theta_{x_1 < x_2 < \cdots < x_N}$, the integrand in Eq. (A2) is symmetric under the exchange of any two variables that are smaller and larger than x_j. By changing the order of the integration variables that are smaller and larger than x_j, we get [57, 58, 64, 71]

$$\mathcal{D}^j_{\substack{n_1, n_2, \cdots, n_N \\ m_1, m_2, \cdots, m_N}} = \sum_{p_1, p_2, \cdots, p_N} \sum_{q_1, q_2, \cdots, q_N} (-1)^{P_{p_1, p_2, \cdots, p_N}} (-1)^{P_{q_1, q_2, \cdots, q_N}} I^j_{\substack{n_{p_1}, n_{p_2}, \cdots, n_{p_N} \\ m_{q_1}, m_{q_2}, \cdots, m_{q_N}}}, \tag{A3}$$

where

$$I^j_{\substack{n_{p_1}, n_{p_2}, \cdots, n_{p_N} \\ m_{q_1}, m_{q_2}, \cdots, m_{q_N}}} = \frac{1}{(j-1)!(N-j)!} \int_{-\infty}^{\infty} dx_j \left[\varphi_{n_{p_j}}(x_j) \varphi_{m_{q_j}}(x_j) e^{2ik_{so}x_j} \times \right.$$
$$\left. \left(\Pi_{k<j} I^{(1)}_{n_{p_k}, m_{q_k}}(x_j) \right) \left(\Pi_{l>j} I^{(2)}_{n_{p_l}, m_{q_l}}(x_j) \right) \right] \tag{A4}$$

with

$$I^{(1)}_{n_{p_k}, m_{q_k}}(x_j) = \int_{-\infty}^{x_j} \varphi_{n_{p_k}}(x) \varphi_{m_{q_k}}(x) dx \tag{A5}$$

and

$$I^{(2)}_{n_{p_l}, m_{q_l}}(x_j) = \int_{x_j}^{\infty} \varphi_{n_{p_l}}(x) \varphi_{m_{q_l}}(x) dx. \tag{A6}$$

According to the generalized Feldheim identity, the product of any number of Hermite polynomials can be expanded into a finite sum of Hermite polynomials [72],

$$H_{N_1}(x) \cdots H_{N_m}(x) = \sum_{\nu_1 \cdots \nu_{m-1}} a_{\nu_1 \cdots \nu_{m-1}} H_M(x), \tag{A7}$$

where

$$M = \sum_{l=1}^{m-1} (N_l - 2\nu_l) + N_m \tag{A8}$$

and

$$a_{\nu_1 \cdots \nu_{m-1}} = \Pi_{l=1}^{m-1} \binom{N_{l+1}}{\nu_l} \binom{\sum_{k=1}^{l-1}(N_k - 2\nu_k + N_l)}{\nu_l} 2^{\nu_l} \nu_l!. \tag{A9}$$

The limits of the summation indices ν_k in Eq. (A7) are given by

$$0 \leq \nu_1 \leq \min\left(N_1, N_2\right), \, 0 \leq \nu_2 \leq \min\left(N_3, N_1 + N_2 - 2\nu_1\right), \cdots, 0 \leq \nu_{m-1} \leq \min\left(N_m, \sum_{k=1}^{m-2}(N_k - 2\nu_k) + N_{m-1}\right). \tag{A10}$$

Using Eqs. (A7)-(A10) to rewrite the product of the two Hermite polynomials contained in $I^{(1)}(x_j)$ and $I^{(2)}(x_j)$, we obtain

$$I^{(1)}_{n_{p_k}, m_{q_k}}(x_j) = N_{n_{p_k}} N_{m_{q_k}} \sum_{\nu_1^{(k)}=0}^{\min(n_{p_k}, m_{q_k})} a_{\nu_1^{(k)}} \int_{-\infty}^{x_j} H_{n_{p_k} + m_{q_k} - 2\nu_1^{(k)}}(x) \exp\left(-x^2\right) dx \tag{A11}$$

and

$$I^{(2)}_{n_{p_l}, m_{q_l}}(x_j) = N_{n_{p_l}} N_{m_{q_l}} \sum_{\nu_1^{(l)}=0}^{\min(n_{p_l}, m_{q_l})} a_{\nu_1^{(l)}} \int_{x_j}^{\infty} H_{n_{p_l} + m_{q_l} - 2\nu_1^{(l)}}(x) \exp\left(-x^2\right) dx. \tag{A12}$$

Instead of working with Eqs. (A11) and (A12) directly, we replace the Hermite polynomials in the integrals using the generating function $g(x,t)$ of the Hermite polynomials,

$$g(x,t) = e^{-t^2 + 2tx} = \sum_{n=0}^{\infty} H_n(x) \frac{t^n}{n!}. \tag{A13}$$

From Eq. (A13), we have

$$H_n(x) = \left.\frac{\partial^n g(x,t)}{\partial t^n}\right|_{t=0}. \tag{A14}$$

Inserting Eq. (A14) into Eqs. (A11)-(A12), we find

$$I^{(1)}_{n_{p_k}, m_{q_k}}(x_j) = N_{n_{p_k}} N_{m_{q_k}} \sum_{\nu_1^{(k)}=0}^{\min(n_{p_k}, m_{q_k})} a_{\nu_1^{(k)}} \frac{\partial^{n_{p_k} + m_{q_k} - 2\nu_1^{(k)}}}{\partial t^{n_{p_k} + m_{q_k} - 2\nu_1^{(k)}}} \left[\int_{-\infty}^{x_j} \exp(-t^2 + 2tx - x^2) dx\right]\Bigg|_{t=0} \tag{A15}$$

and

$$I^{(2)}_{n_{p_l}, m_{q_l}}(x_j) = N_{n_{p_l}} N_{m_{q_l}} \sum_{\nu_1^{(l)}=0}^{\min(n_{p_l}, m_{q_l})} a_{\nu_1^{(l)}} \frac{\partial^{n_{p_l} + m_{q_l} - 2\nu_1^{(l)}}}{\partial t^{n_{p_l} + m_{q_l} - 2\nu_1^{(l)}}} \left[\int_{x_j}^{\infty} \exp(-t^2 + 2tx - x^2) dx\right]\Bigg|_{t=0}. \tag{A16}$$

The key point is that the Gaussian integrals can be calculated analytically. This yields

$$I^{(1)}_{n_{p_k}, m_{q_k}}(x_j) = N_{n_{p_k}} N_{m_{q_k}} \sum_{\nu_1^{(k)}=0}^{\min(n_{p_k}, m_{q_k})} a_{\nu_1^{(k)}} \left[\left(\frac{\sqrt{\pi}}{2} - \frac{\sqrt{\pi}}{2}\mathrm{erf}(x_j)\right) \delta_{n_{p_k} + m_{q_k} - 2\nu_1^{(k)}, 0}\right.$$

$$\left. + \exp(-x_j^2) H_{n_{p_k} + m_{q_k} - 2\nu_1^{(k)} - 1}(x_j)(1 - \delta_{n_{p_k} + m_{q_k} - 2\nu_1^{(k)}, 0})\right] \tag{A17}$$

and

$$I^{(2)}_{n_{p_l}, m_{q_l}}(x_j) = N_{n_{p_l}} N_{m_{q_l}} \sum_{\nu_1^{(l)}=0}^{\min(n_{p_l}, m_{q_l})} a_{\nu_1^{(l)}} \left[\left(\frac{\sqrt{\pi}}{2} + \frac{\sqrt{\pi}}{2}\mathrm{erf}(x_j)\right) \delta_{n_{p_l} + m_{q_l} - 2\nu_1^{(l)}, 0}\right.$$

$$\left. - \exp(-x_j^2) H_{n_{p_l} + m_{q_l} - 2\nu_1^{(l)} - 1}(x_j)(1 - \delta_{n_{p_l} + m_{q_l} - 2\nu_1^{(l)}, 0})\right], \tag{A18}$$

where $\mathrm{erf}(x)$ is the error function,

$$\mathrm{erf}(x) = \frac{2}{\sqrt{\pi}} \int_0^x \exp(-t^2) dt, \tag{A19}$$

and $\delta_{n,m}$ the Kronecker delta function. Plugging Eqs. (A17) and (A18) into Eq. (A4) and rearranging the order of the sums and products, Eq. (A4) can be written as a finite sum over one-dimensional integrals,

$$I^j_{\substack{n_{p_1},n_{p_2},\cdots,n_{p_N} \\ m_{q_1},m_{q_2},\cdots,m_{q_N}}} = \frac{\Pi_{k=1}^N N_{p_k} N_{m_{q_k}}}{(j-1)!(N-j)!} \sum_{\nu_1^{(1)}=0}^{\min(n_{p_1},m_{q_1})} \left\{ a_{\nu_1^{(1)}} \times \cdots \sum_{\nu_1^{(j-1)}=0}^{\min(n_{p_{j-1}},m_{q_{j-1}})} \left\{ a_{\nu_1^{(j-1)}} \times \sum_{\nu_1^{(j+1)}=0}^{\min(n_{p_{j+1}},m_{q_{j+1}})} \left\{ a_{\nu_1^{(j+1)}} \times \right. \right. \right.$$

$$\cdots \sum_{\nu_1^{(N)}=0}^{\min(n_{p_N},m_{q_N})} \left\{ a_{\nu_1^{(N)}} \mathcal{F}^j_{\substack{n_{p_1},n_{p_2},\cdots,n_{p_N} \\ m_{q_1},m_{q_2},\cdots,m_{q_N}}} (\nu_1^{(1)},\cdots,\nu_1^{(j-1)},\nu_1^{(j+1)},\cdots,\nu_1^{(N)}) \right\} \cdots \left. \right\} \left. \right\} \cdots \left. \right\}, \tag{A20}$$

where

$$\mathcal{F}^j_{\substack{n_{p_1},n_{p_2},\cdots,n_{p_N} \\ m_{q_1},m_{q_2},\cdots,m_{q_N}}} (\nu_1^{(1)},\cdots,\nu_1^{(j-1)},\nu_1^{(j+1)},\cdots,\nu_1^{(N)}) = \int_{-\infty}^{\infty} H_{n_{p_j}}(x_j) H_{m_{q_j}}(x_j) \exp(2ik_{so}x_j - x_j^2) \times$$

$$\Pi_{k<j} \left[\left(\frac{\sqrt{\pi}}{2} - \frac{\sqrt{\pi}}{2}\mathrm{erf}(x_j) \right) \delta_{n_{p_k}+m_{q_k}-2\nu_1^{(k)},0} + \exp(-x_j^2) H_{n_{p_k}+m_{q_k}-2\nu_1^{(k)}-1}(x_j)(1 - \delta_{n_{p_k}+m_{q_k}-2\nu_1^{(k)},0}) \right] \times$$

$$\Pi_{l>j} \left[\left(\frac{\sqrt{\pi}}{2} + \frac{\sqrt{\pi}}{2}\mathrm{erf}(x_j) \right) \delta_{n_{p_l}+m_{q_l}-2\nu_1^{(l)},0} - \exp(-x_j^2) H_{n_{p_l}+m_{q_l}-2\nu_1^{(l)}-1}(x_j)(1 - \delta_{n_{p_l}+m_{q_l}-2\nu_1^{(l)},0}) \right] dx_j. \tag{A21}$$

To simplify the notation, we define the index function $d(k)$,

$$d(k) = n_{p_k} + m_{q_k} - 2\nu_1^{(k)}. \tag{A22}$$

For $k < j$ and $l > j$, we use $k_1, k_2, \cdots, k_{\mathcal{K}}$ and $l_1, l_2, \cdots, l_{\mathcal{L}}$, respectively, to indicate all the $k's$ and $l's$ that make $d(k)$ and $d(l)$ non-zero ($0 \le \mathcal{K} \le j-1$ and $0 \le \mathcal{L} \le N-j$). Then Eq. (A21) becomes

$$\mathcal{F}^j_{\substack{n_{p_1},n_{p_2},\cdots,n_{p_N} \\ m_{q_1},m_{q_2},\cdots,m_{q_N}}} (\nu_1^{(1)},\cdots,\nu_1^{(j-1)},\nu_1^{(j+1)},\cdots,\nu_1^{(N)}) =$$

$$\int_{-\infty}^{\infty} H_{n_{p_j}}(x_j) H_{m_{q_j}}(x_j) \exp\left[2ik_{so}x_j - (\mathcal{K}+\mathcal{L}+1)x_j^2 \right] (-1)^{\mathcal{L}} \left(\frac{\sqrt{\pi}}{2} - \frac{\sqrt{\pi}}{2}\mathrm{erf}(x_j) \right)^{j-1-\mathcal{K}} \left(\frac{\sqrt{\pi}}{2} + \frac{\sqrt{\pi}}{2}\mathrm{erf}(x_j) \right)^{N-j-\mathcal{L}} \times$$

$$H_{d(k_1)-1}(x_j) \cdots H_{d(k_{\mathcal{K}})-1}(x_j) H_{d(l_1)-1}(x_j) \cdots H_{d(l_{\mathcal{L}})-1}(x_j) dx_j. \tag{A23}$$

Expanding the $\left(\frac{\sqrt{\pi}}{2} - \frac{\sqrt{\pi}}{2}\mathrm{erf}(x_j) \right)^{j-1-\mathcal{K}}$ and $\left(\frac{\sqrt{\pi}}{2} + \frac{\sqrt{\pi}}{2}\mathrm{erf}(x_j) \right)^{N-j-\mathcal{L}}$ terms, Eq. (A23) becomes

$$\mathcal{F}^j_{\substack{n_{p_1},n_{p_2},\cdots,n_{p_N} \\ m_{q_1},m_{q_2},\cdots,m_{q_N}}} (\nu_1^{(1)},\cdots\nu_1^{(j-1)},\nu_1^{(j+1)},\cdots\nu_1^{(N)}) =$$

$$\left(\frac{\sqrt{\pi}}{2} \right)^{N-\mathcal{L}-\mathcal{K}-1} (-1)^{\mathcal{L}} \sum_{r=0}^{j-1-\mathcal{K}} \sum_{s=0}^{N-j-\mathcal{L}} \binom{j-1-\mathcal{K}}{r} \binom{N-j-\mathcal{L}}{s} (-1)^r \times \int_{-\infty}^{\infty} \exp\left[2ik_{so}x_j - (\mathcal{K}+\mathcal{L}+1)x_j^2 \right] [\mathrm{erf}(x_j)]^{r+s} \times$$

$$H_{n_{p_j}}(x_j) H_{m_{q_j}}(x_j) H_{d(k_1)-1}(x_j) \cdots H_{d(k_{\mathcal{K}})-1}(x_j) H_{d(l_1)-1}(x_j) \cdots H_{d(l_{\mathcal{L}})-1}(x_j) dx_j. \tag{A24}$$

Equation (A24) contains a product of Hermite polynomials, which can be converted into a finite sum of Hermite polynomials according to the Feldheim identity,

$$H_{n_{p_j}}(x_j) H_{m_{q_j}}(x_j) H_{d(k_1)-1}(x_j) \cdots H_{d(k_{\mathcal{K}})-1}(x_j) H_{d(l_1)-1}(x_j) \cdots H_{d(l_{\mathcal{L}})-1}(x_j) = \sum_{\nu_1 \cdots \nu_{\mathcal{L}+\mathcal{K}+1}} a_{\nu_1 \cdots \nu_{\mathcal{L}+\mathcal{K}+1}} H_M(x_j), \tag{A25}$$

where the coefficients $a_{\nu_1 \cdots \nu_{\mathcal{L}+\mathcal{K}+1}}$ and the relationship between M and the indices $n_{p_j}, m_{q_j}, d(k_1), \cdots, d(l_{\mathcal{L}})$ are defined in Eqs. (A8)-(A10).

Plugging Eq. (A25) into Eq. (A24), we find

$$
\mathcal{F}^{j}_{\substack{n_{p_1}, n_{p_2}, \cdots, n_{p_N} \\ m_{q_1}, m_{q_2}, \cdots, m_{q_N}}} (\nu_1^{(1)}, \cdots, \nu_1^{(j-1)}, \nu_1^{(j+1)}, \cdots, \nu_1^{(N)}) =
$$

$$
\left(\frac{\sqrt{\pi}}{2} \right)^{N-\mathcal{L}-\mathcal{K}-1} (-1)^{\mathcal{L}} \sum_{r=0}^{j-1-\mathcal{K}} \sum_{s=0}^{N-j-\mathcal{L}} \binom{j-1-\mathcal{K}}{r} \binom{N-j-\mathcal{L}}{s} (-1)^r \sum_{\nu_1 \cdots \nu_{\mathcal{L}+\mathcal{K}+1}} a_{\nu_1 \cdots \nu_{\mathcal{L}+\mathcal{K}+1}} \mathcal{G}^{M}_{(r+s;\mathcal{K}+\mathcal{L})}, \quad \text{(A26)}
$$

where

$$
\mathcal{G}^{M}_{(r+s;\mathcal{K}+\mathcal{L})} = \int_{-\infty}^{\infty} \exp\left[2ik_{so}x_j - (\mathcal{K}+\mathcal{L}+1)x_j^2 \right] \left[\text{erf}(x_j) \right]^{r+s} H_M(x_j) dx_j. \quad \text{(A27)}
$$

We call $\mathcal{G}^{M}_{(r+s;\mathcal{K}+\mathcal{L})}$ the $\mathcal{G}$ integral of the order $r+s$. The $\mathcal{G}$ integral of order 0 can be evaluated analytically,

$$
\mathcal{G}^{M}_{(0,\mathcal{K}+\mathcal{L})} = \frac{\sqrt{\pi}}{\sqrt{\mathcal{K}+\mathcal{L}+1}} \exp\left(-\frac{k_{so}^2}{\mathcal{K}+\mathcal{L}+1} \right) H_M \left(\frac{2ik_{so}}{\sqrt{(\mathcal{K}+\mathcal{L}+1)(\mathcal{K}+\mathcal{L})}} \right) \left(\frac{\mathcal{K}+\mathcal{L}}{\mathcal{K}+\mathcal{L}+1} \right)^{M/2}. \quad \text{(A28)}
$$

To evaluate $\mathcal{G}^{M}_{(r+s;\mathcal{K}+\mathcal{L})}$ of higher order, we develop an iterative procedure, in which the $\mathcal{G}$ integral of order $r+s$ is written in terms of $\mathcal{G}$ integrals of order $r+s-1$. Since the $r+s=0$ integral is known, this allows for the evaluation of the $\mathcal{G}$ integral of arbitrary order. Using the generating function of the Hermite polynomials, we have

$$
\mathcal{G}^{M}_{(r+s;\mathcal{K}+\mathcal{L})} = \left\{ \frac{\partial^M}{\partial t^M} \int_{-\infty}^{\infty} \exp\left[2(ik_{so}+t)x_j - (\mathcal{K}+\mathcal{L}+1)x_j^2 - t^2 \right] \left[\text{erf}(x_j) \right]^{r+s} dx_j \right\} \Bigg|_{t=0}. \quad \text{(A29)}
$$

Using integration by parts, Eq. (A29) becomes

$$
\mathcal{G}^{M}_{(r+s;\mathcal{K}+\mathcal{L})} = \left\{ \frac{\partial^M}{\partial t^M} \left[g^{(1)}_{(r+s,\mathcal{K}+\mathcal{L})} - g^{(2)}_{(r+s,\mathcal{K}+\mathcal{L})} \right] \right\} \Bigg|_{t=0}, \quad \text{(A30)}
$$

where

$$
g^{(1)}_{(r+s,\mathcal{K}+\mathcal{L})} = \mathcal{H}(k_{so}, \mathcal{K}, \mathcal{L}; t, x_j) \left[\text{erf}(x_j) \right]^{r+s} \big|_{x_j=-\infty}^{x_j=\infty} \quad \text{(A31)}
$$

and

$$
g^{(2)}_{(r+s,\mathcal{K}+\mathcal{L})} = (r+s) \frac{2}{\sqrt{\pi}} \int_{-\infty}^{\infty} \mathcal{H}(k_{so}, \mathcal{K}, \mathcal{L}; t, x_j) \left[\text{erf}(x_j) \right]^{r+s-1} \exp(-x_j^2) dx_j \quad \text{(A32)}
$$

with

$$
\mathcal{H}(k_{so}, \mathcal{K}, \mathcal{L}; t, x_j) = \int_0^{x_j} \exp\left[2(ik_{so}+t)x - (\mathcal{K}+\mathcal{L}+1)x^2 - t^2 \right] dx. \quad \text{(A33)}
$$

The Gaussian integral in Eq. (A33) can be calculated analytically,

$$
\mathcal{H}(k_{so}, \mathcal{K}, \mathcal{L}; t, x_j) = \frac{\sqrt{\pi}}{2\sqrt{\mathcal{K}+\mathcal{L}+1}} \exp\left[-\frac{k_{so}^2 - 2ik_{so}t + (\mathcal{K}+\mathcal{L})t^2}{\mathcal{K}+\mathcal{L}+1} \right] \text{erf}\left[\frac{-ik_{so} - t + (\mathcal{K}+\mathcal{L}+1)x_j}{\sqrt{\mathcal{K}+\mathcal{L}+1}} \right]. \quad \text{(A34)}
$$

Using that the value of the error function $\text{erf}(x)$ at infinity is known, $\text{erf}(\pm\infty) = \pm 1$, $g^{(1)}_{(r+s,\mathcal{K}+\mathcal{L})}$ evaluates to

$$
g^{(1)}_{(r+s,\mathcal{K}+\mathcal{L})} = \frac{\sqrt{\pi}}{2\sqrt{\mathcal{K}+\mathcal{L}+1}} \exp\left[-\frac{k_{so}^2 - 2ik_{so}t + (\mathcal{K}+\mathcal{L})t^2}{\mathcal{K}+\mathcal{L}+1} \right] \left[1 - (-1)^{r+s+1} \right]. \quad \text{(A35)}
$$

Inserting Eq. (A34) into Eq. (A32), we have

$$
g^{(2)}_{(r+s,\mathcal{K}+\mathcal{L})} = (r+s) \frac{\exp\left[-\frac{k_{so}^2 - 2ik_{so}t + (\mathcal{K}+\mathcal{L})t^2}{\mathcal{K}+\mathcal{L}+1} \right]}{\sqrt{\mathcal{K}+\mathcal{L}+1}} \left\{ \int_{-\infty}^{\infty} \text{erf}\left[\frac{-ik_{so} - t + (\mathcal{K}+\mathcal{L}+1)x_j}{\sqrt{\mathcal{K}+\mathcal{L}+1}} \right] \left[\text{erf}(x_j) \right]^{r+s-1} \exp(-x_j^2) dx_j \right\}. \quad \text{(A36)}
$$

Next, we expand $g^{(1)}_{(r+s,\mathcal{K}+\mathcal{L})}$ and $g^{(2)}_{(r+s,\mathcal{K}+\mathcal{L})}$ in terms of t up to power M and evaluate the Mth derivative with respect to t at $t=0$. For $\mathcal{K}+\mathcal{L} \neq 0$, the exponential in Eq. (A35) can be interpreted as a generating function of the Hermite polynomials. Expanding this term into a sum of Hermite polynomials, we find

$$
g^{(1)}_{(r+s,\mathcal{K}+\mathcal{L})} =
$$

$$
\frac{\sqrt{\pi}}{2\sqrt{\mathcal{K}+\mathcal{L}+1}} \left[1 - (-1)^{r+s+1}\right] \exp\left[-\frac{k_{so}^2}{\mathcal{K}+\mathcal{L}+1} + \frac{2ik_{so}}{\sqrt{(\mathcal{K}+\mathcal{L}+1)(\mathcal{K}+\mathcal{L})}}\left(\sqrt{\frac{\mathcal{K}+\mathcal{L}}{\mathcal{K}+\mathcal{L}+1}}t\right) - \left(\sqrt{\frac{\mathcal{K}+\mathcal{L}}{\mathcal{K}+\mathcal{L}+1}}t\right)^2\right]
$$

$$
= \frac{\sqrt{\pi}}{2\sqrt{\mathcal{K}+\mathcal{L}+1}} \left[1 - (-1)^{r+s+1}\right] \exp\left(-\frac{k_{so}^2}{\mathcal{K}+\mathcal{L}+1}\right) \left[\sum_{n=0}^{\infty} H_n\left(\frac{2ik_{so}}{\sqrt{(\mathcal{K}+\mathcal{L}+1)(\mathcal{K}+\mathcal{L})}}\right) \frac{\left(\sqrt{\frac{\mathcal{K}+\mathcal{L}}{\mathcal{K}+\mathcal{L}+1}}t\right)^n}{n!}\right]. \quad (A37)
$$

For $\mathcal{K}+\mathcal{L}=0$, the power series of $g^{(1)}_{(r+s,\mathcal{K}+\mathcal{L})}$ in terms of t is

$$
g^{(1)}_{(r+s,\mathcal{K}+\mathcal{L})} = \frac{\sqrt{\pi}}{2\sqrt{\mathcal{K}+\mathcal{L}+1}} \left[1 - (-1)^{r+s+1}\right] \exp\left(-k_{so}^2\right) \left[\sum_{n=0}^{\infty} \frac{(2ik_{so}t)^n}{n!}\right]. \quad (A38)
$$

This can be understood as the limiting result of Eq. (A37),

$$
\lim_{\mathcal{K}+\mathcal{L}\to 0} H_n\left(\frac{2ik_{so}}{\sqrt{(\mathcal{K}+\mathcal{L}+1)(\mathcal{K}+\mathcal{L})}}\right) \left(\frac{\mathcal{K}+\mathcal{L}}{\mathcal{K}+\mathcal{L}+1}\right)^{n/2} = (2ik_{so})^n. \quad (A39)
$$

In what follows, we take this limit when $\mathcal{K}+\mathcal{L}=0$. The derivative of $g^{(1)}_{(r+s;\mathcal{K}+\mathcal{L})}$ with respect to t at $t=0$ is then

$$
\left(\frac{\partial^M}{\partial t^M} g^{(1)}_{(r+s;\mathcal{K}+\mathcal{L})}\right)\bigg|_{t=0} =
$$

$$
\frac{\sqrt{\pi}}{2\sqrt{\mathcal{K}+\mathcal{L}+1}} \exp\left(-\frac{k_{so}^2}{\mathcal{K}+\mathcal{L}+1}\right) H_M\left(\frac{2ik_{so}}{\sqrt{(\mathcal{K}+\mathcal{L}+1)(\mathcal{K}+\mathcal{L})}}\right) \left(\frac{\mathcal{K}+\mathcal{L}}{\mathcal{K}+\mathcal{L}+1}\right)^{M/2} \left[1 - (-1)^{r+s+1}\right]. \quad (A40)
$$

To evaluate $g^{(2)}_{(r+s,\mathcal{K}+\mathcal{L})}$, we notice that it can be written in the form $g^{(1)}_{(r+s,\mathcal{K}+\mathcal{L})} \int \mathrm{erf}(\cdots) dx_j$. The expansion of $g^{(1)}_{(r+s,\mathcal{K}+\mathcal{L})}$ is given in Eq. (A37). An additional t-dependence enters through the error function in the integrand in Eq. (A36). Rewriting the error function in a series in t, we have

$$
\mathrm{erf}\left(\frac{-ik_{so} - t + (\mathcal{K}+\mathcal{L}+1)x_j}{\sqrt{\mathcal{K}+\mathcal{L}+1}}\right) = \mathrm{erf}\left(\sqrt{\mathcal{K}+\mathcal{L}+1}x_j - \frac{ik_{so}}{\sqrt{\mathcal{K}+\mathcal{L}+1}}\right) - \frac{2}{\sqrt{\pi}} \exp\left(\frac{k_{so}^2}{\mathcal{K}+\mathcal{L}+1}\right) \times
$$

$$
\sum_{n=1}^{\infty} \exp\left[2ik_{so}x_j - (\mathcal{K}+\mathcal{L}+1)x_j^2\right] H_n\left(\sqrt{\mathcal{K}+\mathcal{L}+1}x_j - \frac{ik_{so}}{\sqrt{\mathcal{K}+\mathcal{L}+1}}\right) \left(\frac{t}{\sqrt{\mathcal{K}+\mathcal{L}+1}}\right)^n \frac{1}{n!}. \quad (A41)
$$

Using the multiplication theorem [73]

$$
H_n(\alpha x) = \sum_{v=0}^{[\frac{n}{2}]} \alpha^{n-2v}(\alpha^2 - 1)^v \binom{n}{2v} \frac{(2v)!}{v!} H_{n-2v}(x) \quad (A42)
$$

and the addition theorem [74]

$$
H_n(x + y) = \sum_{w=0}^{n} \binom{n}{w} H_w(x)(2y)^{n-w}, \quad (A43)
$$

where $[\frac{n}{2}]$ denotes the integer part of $n/2$, the Hermite polynomial on the right hand side of Eq. (A41) can be expanded into a finite sum over products of Hermite polynomials in which the dependence on x_j has been "isolated",

$$H_n\left(\sqrt{\mathcal{K}+\mathcal{L}+1}\,x_j - \frac{ik_{so}}{\sqrt{\mathcal{K}+\mathcal{L}+1}}\right) =$$

$$\sum_{v=0}^{[\frac{n}{2}]}\sum_{w=0}^{n-2v}(\mathcal{K}+\mathcal{L}+1)^{\frac{n-2v}{2}}(\mathcal{K}+\mathcal{L})^v\binom{n}{2v}\frac{(2v)!}{v!}\binom{n-2v}{w}H_w\left(\frac{2ik_{so}}{\mathcal{K}+\mathcal{L}+1}\right)H_{n-2v-w}(x_j). \quad \text{(A44)}$$

For $\mathcal{K}+\mathcal{L}=0$, Eq. (A44) contains an indeterminate term 0^0 which is understood to be 1. In this case, Eq. (A44) becomes

$$H_n\left(x_j - ik_{so}\right) = \sum_{w=0}^{n}\binom{n}{w}H_w\left(2ik_{so}\right)H_{n-w}(x_j). \quad \text{(A45)}$$

Using Eqs. (A37), (A41) and (A44), Eq. (A36) becomes

$$g^{(2)}_{(r+s;\mathcal{K}+\mathcal{L})} =$$

$$\sum_{n=0}^{\infty}\left\{\frac{r+s}{\sqrt{\mathcal{K}+\mathcal{L}+1}}\exp\left(-\frac{k_{so}^2}{\mathcal{K}+\mathcal{L}+1}\right)\left[H_n\left(\frac{2ik_{so}}{\sqrt{(\mathcal{K}+\mathcal{L}+1)(\mathcal{K}+\mathcal{L})}}\right)\left(\frac{\mathcal{K}+\mathcal{L}}{\mathcal{K}+\mathcal{L}+1}\right)^{n/2}\mathcal{I}_{(r+s-1,\mathcal{K}+\mathcal{L})}\right]+\right.$$

$$\frac{2(r+s)}{\sqrt{\pi}(\mathcal{K}+\mathcal{L}+1)^{\frac{n+1}{2}}}\sum_{u=0}^{n}\sum_{v=0}^{[\frac{u}{2}]}\sum_{w=0}^{u-2v}H_{n-u}\left(\frac{2ik_{so}}{\sqrt{(\mathcal{K}+\mathcal{L}+1)(\mathcal{K}+\mathcal{L})}}\right)(\mathcal{K}+\mathcal{L})^{\frac{n-u}{2}+v}(\mathcal{K}+\mathcal{L}+1)^{\frac{u-2v}{2}}\times$$

$$\left.\binom{n}{u}\binom{u}{2v}\binom{u-2v}{w}\frac{(2v)!}{v!}H_w\left(\frac{2ik_{so}}{\mathcal{K}+\mathcal{L}+1}\right)\mathcal{G}^{(u-2v-w)}_{(r+s-1,\mathcal{K}+\mathcal{L}+1)}\right\}\frac{t^n}{n!}, \quad \text{(A46)}$$

where

$$\mathcal{I}_{(r+s-1,\mathcal{K}+\mathcal{L})} = \int_{-\infty}^{\infty}\text{erf}\left(\sqrt{\mathcal{K}+\mathcal{L}+1}\,x_j - \frac{ik_{so}}{\sqrt{\mathcal{K}+\mathcal{L}+1}}\right)[\text{erf}(x_j)]^{r+s-1}\exp(-x_j^2)dx_j. \quad \text{(A47)}$$

The Mth derivative of $g^{(2)}_{(r+s;\mathcal{K}+\mathcal{L})}$ with respect to t at $t=0$ is then

$$\left(\frac{\partial^M}{\partial t^M}g^{(2)}_{(r+s;\mathcal{K}+\mathcal{L})}\right)\bigg|_{t=0} = g^{(2,1)}_{(r+s,\mathcal{K}+\mathcal{L})} + g^{(2,2)}_{(r+s,\mathcal{K}+\mathcal{L})}, \quad \text{(A48)}$$

where

$$g^{(2,1)}_{(r+s,\mathcal{K}+\mathcal{L})} =$$

$$\frac{r+s}{\sqrt{\mathcal{K}+\mathcal{L}+1}}\exp\left(-\frac{k_{so}^2}{\mathcal{K}+\mathcal{L}+1}\right)H_M\left(\frac{2ik_{so}}{\sqrt{(\mathcal{K}+\mathcal{L}+1)(\mathcal{K}+\mathcal{L})}}\right)\left(\frac{\mathcal{K}+\mathcal{L}}{\mathcal{K}+\mathcal{L}+1}\right)^{M/2}\mathcal{I}_{(r+s-1,\mathcal{K}+\mathcal{L})} \quad \text{(A49)}$$

and

$$g^{(2,2)}_{(r+s,\mathcal{K}+\mathcal{L})} = \frac{2(r+s)}{\sqrt{\pi}(\mathcal{K}+\mathcal{L}+1)^{\frac{M+1}{2}}}\sum_{u=0}^{M}\sum_{v=0}^{[\frac{u}{2}]}\sum_{w=0}^{u-2v}H_{M-u}\left(\frac{2ik_{so}}{\sqrt{(\mathcal{K}+\mathcal{L}+1)(\mathcal{K}+\mathcal{L})}}\right)(\mathcal{K}+\mathcal{L})^{\frac{M-u}{2}+v}(\mathcal{K}+\mathcal{L}+1)^{\frac{u-2v}{2}}\times$$

$$\binom{M}{u}\binom{u}{2v}\binom{u-2v}{w}\frac{(2v)!}{v!}H_w\left(\frac{2ik_{so}}{\mathcal{K}+\mathcal{L}+1}\right)\mathcal{G}^{(u-2v-w)}_{(r+s-1,\mathcal{K}+\mathcal{L}+1)}. \quad \text{(A50)}$$

To evaluate the integral $\mathcal{I}_{(r+s-1,\mathcal{K}+\mathcal{L})}$, we integrate by parts. Using

$$\int_0^{x_j}[\text{erf}(x)]^{r+s-1}\exp(-x^2)dx = \frac{\sqrt{\pi}\,[\text{erf}(x_j)]^{r+s}}{2(r+s)} \quad \text{(A51)}$$

and

$$\left[\mathrm{erf}\left(\sqrt{\mathcal{K}+\mathcal{L}+1}x_j - \frac{ik_{so}}{\sqrt{\mathcal{K}+\mathcal{L}+1}}\right)\frac{\sqrt{\pi}\,[\mathrm{erf}(x_j)]^{r+s}}{2(r+s)}\right]\Bigg|_{x_j=-\infty}^{x_j=\infty} = \frac{\sqrt{\pi}}{2(r+s)}\left[1-(-1)^{r+s+1}\right], \qquad (A52)$$

we find

$$\mathcal{I}_{(r+s-1,\mathcal{K}+\mathcal{L})} = \frac{\sqrt{\pi}}{2(r+s)}\left[1-(-1)^{r+s+1}\right] - \frac{\sqrt{\mathcal{K}+\mathcal{L}+1}\exp\left(\frac{k_{so}^2}{\mathcal{K}+\mathcal{L}+1}\right)}{r+s}\mathcal{J}_{(r+s,\mathcal{K}+\mathcal{L})}, \qquad (A53)$$

where

$$\mathcal{J}_{(r+s,\mathcal{K}+\mathcal{L})} = \int_{-\infty}^{\infty} [\mathrm{erf}(x_j)]^{r+s}\exp[-(\mathcal{K}+\mathcal{L}+1)x_j^2 + 2ik_{so}x_j]dx_j. \qquad (A54)$$

Using Eq. (A53) in Eq. (A49) and using Eq. (A40), we find

$$\mathcal{G}_{(r+s;\mathcal{K}+\mathcal{L})}^M = \mathcal{J}_{(r+s,\mathcal{K}+\mathcal{L})} - g_{(r+s,\mathcal{K}+\mathcal{L})}^{(2,2)}. \qquad (A55)$$

Our manipulations have reduced $\mathcal{G}_{(r+s;\mathcal{K}+\mathcal{L})}^M$ to an expression that contains two types of one-dimensional integrals. The first one, $\mathcal{J}_{(r+s,\mathcal{K}+\mathcal{L})}$, only depends on k_{so}, $\mathcal{K}$ and $\mathcal{L}$, implying that only a few of these integrals need to be calculated for a given k_{so}. For $r+s=1$, $\mathcal{J}_{(1,\mathcal{K}+\mathcal{L})}$ can be calculated analytically,

$$\mathcal{J}_{(1,\mathcal{K}+\mathcal{L})} = \sqrt{\frac{\pi}{\mathcal{K}+\mathcal{L}+1}}\exp\left(-\frac{k_{so}^2}{\mathcal{K}+\mathcal{L}+1}\right)\mathrm{erf}\left[\frac{ik_{so}}{\sqrt{(\mathcal{K}+\mathcal{L}+1)(\mathcal{K}+\mathcal{L}+2)}}\right]. \qquad (A56)$$

For $r+s>1$, $\mathcal{J}_{(1,\mathcal{K}+\mathcal{L})}$ can be calculated numerically with essentially arbitrary accuracy. The second integral, $\mathcal{G}_{(r+s-1;\mathcal{K}+\mathcal{L}+1)}^{u-2v-w}$ (the $\mathcal{G}$ integral of order $r+s-1$), is contained in $g_{(r+s,\mathcal{K}+\mathcal{L})}^{(2,2)}$. To see the iterative structure of our result more clearly, we rewrite Eq. (A55) as

$$\mathcal{G}_{(r+s;\mathcal{K}+\mathcal{L})}^M = \mathcal{J}_{(r+s,\mathcal{K}+\mathcal{L})} - \sum_j c_j \mathcal{G}_{(r+s-1;\mathcal{K}+\mathcal{L}+1)}^{u-2v-w}, \qquad (A57)$$

where j runs over all combinations of allowed indices and c_j contains all the prefactors [the c_j can be read off Eq. (A50)]. Thus, to determine the $\mathcal{G}$ integral of order $r+s$, a finite number of $\mathcal{G}$ integrals of order $r+s-1$ is needed. To evaluate the $\mathcal{G}$ integral of order $r+s-1$, a finite number of $\mathcal{G}$ integrals of order $r+s-2$ is needed, and so on. Since the $\mathcal{G}$ integral of order 0 is known analytically [see Eq. (A28)], the $\mathcal{G}$ integral of arbitrary order can be obtained iteratively. It should be noted that the $\mathcal{G}$ integral of order 1 has an analytical result since $\mathcal{G}_{(0,\mathcal{K}+\mathcal{L})}$ and $\mathcal{J}_{(1,\mathcal{K}+\mathcal{L})}$ are known analytically.

In summary, first we calculate, using Eq. (A54), all the $\mathcal{J}$ integrals needed for the evaluation of the $\mathcal{G}$ integrals. Secondly, using the values of the $\mathcal{J}$ integrals, the required $\mathcal{G}$ integrals are calculated iteratively based on Eq. (A55). Thirdly, plugging the values of the $\mathcal{G}$ integrals into Eq. (A26), the $\mathcal{F}$ integrals with arguments $\nu_1^{(1)}, \cdots, \nu_1^{(j-1)}, \nu_1^{(j+1)}, \cdots, \nu_1^{(N)}$ are obtained. Forthly, plugging the values of the $\mathcal{F}$ integrals into Eq. (A20), the I integrals can be calculated. Finally, plugging the values of the I integrals into Eq. (A3), we obtain the values of the $\mathcal{D}$ integrals. The sums in the above expressions are all finite. As a result, the only error in evaluating the $\mathcal{D}$ integrals comes from the numerical evaluation of the one-dimensional $\mathcal{J}$ integrals. Everything is analytical for $N=2$ while one and three $\mathcal{J}$ integrals have to be evaluated numerically for $N=3$ and 4, respectively. The reader may wonder why we choose the outlined iterative procedure for evaluating the one-dimensional integral given in Eq. (A27) over an evaluation of Eq. (A27) by direct numerical integration. The answer is two-fold. First, Eq. (A27) has to be evaluated for Hermite polynomials of different orders; the numerical integrals required in our iterative procedure, in contrast, are independent of the M quantum number. Second, for large M, the integrand in Eq. (A27) is highly oscillatory, making the one-dimensional integration somewhat non-trivial.

To be concrete, we discuss how to apply the formalism to the three particle system. In this case, the $\mathcal{D}$ integral depends on j ($j=1,2,3$) and the quantum numbers n_1, n_2, n_3, m_1, m_2, and m_3. For a fixed j, there are $3! \times 3! = 36$ terms (I integrals) in the sum on the right hand side of Eq. (A3). For each I integral, we have a double sum on the right hand side of Eq. (A20). For $j=2$, e.g., the summation dummies are $\nu_1^{(1)}$ and $\nu_1^{(3)}$. Correspondingly, the $\mathcal{F}$ integrals have two arguments. The indices $\mathcal{K}$ and $\mathcal{L}$ in Eq. (A23) satisfy $0 \leq \mathcal{K} \leq 1$ and $0 \leq \mathcal{L} \leq 1$. As

a result, the indices r and s defined in Eq. (A24) satisfy $0 \leq r \leq 1$ and $0 \leq s \leq 1$ with the additional constraint $r + s \leq N - 1 - \mathcal{K} - \mathcal{L}$, which is due to the limits $r \leq j - \mathcal{K} - 1$ and $s \leq N - \mathcal{L} - j$ in the sums on the right hand side of Eq. (A24). Thus, the allowed $(r + s, \mathcal{K} + \mathcal{L})$ combinations are $(2, 0), (1, 0), (0, 0), (1, 1), (0, 1), (0, 2)$. Since the number of Hermite polynomials in the product in Eq. (A24) is $\mathcal{K} + \mathcal{L} + 2$, which is less or equal to 4 (since $0 \leq \mathcal{K} \leq 1$ and $0 \leq \mathcal{L} \leq 1$), the coefficients on the right hand side of Eq. (A25) have at most three indices.

Appendix B: Expressions for $\langle S_x(x) \rangle$ and $\langle S_z(x) \rangle$ for $N = 3 - 4$

For $N = 3$, the expressions for C_{1x}, C_{2x}, and C_z in Eqs. (47)-(48) in terms of the coefficients $C_1 - C_4$ in Eq. (46) are

$$C_{1x} = (C_1 - C_3)^* (C_2 + C_4) + (C_1 - C_3)(C_2 + C_4)^*, \tag{B1}$$

$$C_{2x} = C_1^* C_3 + C_1 C_3^* - |C_2|^2 - |C_4|^2, \tag{B2}$$

and

$$C_z = i[(C_1 - C_3)^* (C_2 - C_4) - (C_1 - C_3)(C_2 - C_4)^*]. \tag{B3}$$

The expressions for $n_{1x}(x), n_{2x}(x)$, and $n_z(x)$ in Eqs. (47)-(48) are

$$n_{1x}(x) = \int_{-\infty}^{\infty} |D(0, 1, 2)|^2 \Theta_{x_1 < x_2 < x_3} [\delta(x - x_1) + \delta(x - x_3)] d\vec{x}, \tag{B4}$$

$$n_{2x}(x) = \int_{-\infty}^{\infty} |D(0, 1, 2)|^2 \Theta_{x_1 < x_2 < x_3} \delta(x - x_2) d\vec{x}, \tag{B5}$$

and

$$n_z(x) = \int_{-\infty}^{\infty} |D(0, 1, 2)|^2 \Theta_{x_1 < x_2 < x_3} [\delta(x - x_1) - \delta(x - x_3)] d\vec{x}. \tag{B6}$$

For $N = 4$, the expressions for C_{1x}, C_{2x}, C_{1z}, and C_{2z} in Eqs. (50)-(51) in terms of the coefficients $C_1 - C_{10}$ in Eq. (49) are

$$\begin{aligned} C_{1x} = \frac{1}{2} \left[(C_2 + C_5)(C_1 + C_8)^* + (C_2 + C_5)^* (C_1 + C_8) \right] \\ + \frac{1}{\sqrt{2}} \left[C_3 (C_{10} + C_6)^* + C_3^* (C_{10} + C_6) + C_4 (C_7 + C_9)^* + C_4^* (C_7 + C_9) \right], \end{aligned} \tag{B7}$$

$$\begin{aligned} C_{2x} = \frac{1}{2} \left[(C_3 + C_4)(C_1 + C_8)^* + (C_3 + C_4)^* (C_1 + C_8) \right] \\ + \frac{1}{\sqrt{2}} \left[C_5 (C_9 + C_{10})^* + C_5^* (C_9 + C_{10}) + C_2 (C_6 + C_7)^* + C_2^* (C_6 + C_7) \right], \end{aligned} \tag{B8}$$

$$\begin{aligned} C_{1z} = \frac{i}{2} \left[(C_2 - C_5)(C_1 + C_8)^* - (C_2 - C_5)^* (C_1 + C_8) \right] \\ + \frac{i}{\sqrt{2}} \left[C_3 (C_{10} - C_6)^* - C_3^* (C_{10} - C_6) + C_4 (C_9 - C_7)^* - C_4^* (C_9 - C_7) \right], \end{aligned} \tag{B9}$$

and

$$\begin{aligned} C_{2z} = \frac{i}{2} \left[(C_3 - C_4)(C_1 + C_8)^* - (C_3 - C_4)^* (C_1 + C_8) \right] \\ + \frac{i}{\sqrt{2}} \left[C_5 (C_9 - C_{10})^* - C_5^* (C_9 - C_{10}) + C_2 (C_7 - C_6)^* - C_2^* (C_7 - C_6) \right]. \end{aligned} \tag{B10}$$

The expressions for $n_{1x}(x), n_{2x}(x), n_{1z}(x),$ and $n_{2z}(x)$ in Eqs. (50)-(51) are

$$n_{1x}(x) = \int_{-\infty}^{\infty} |D(0,1,2,4)|^2 \Theta_{x_1<x_2<x_3<x_4} \left[\delta(x-x_1) + \delta(x-x_4)\right] d\vec{x}, \tag{B11}$$

$$n_{2x}(x) = \int_{-\infty}^{\infty} |D(0,1,2,4)|^2 \Theta_{x_1<x_2<x_3<x_4} [\delta(x-x_2) + \delta(x-x_3)] d\vec{x}, \tag{B12}$$

$$n_{1z}(x) = \int_{-\infty}^{\infty} |D(0,1,2,4)|^2 \Theta_{x_1<x_2<x_3<x_4} [\delta(x-x_1) - \delta(x-x_4)] d\vec{x}, \tag{B13}$$

and

$$n_{2z}(x) = \int_{-\infty}^{\infty} |D(0,1,2,4)|^2 \Theta_{x_1<x_2<x_3<x_4} [\delta(x-x_2) - \delta(x-x_3)] d\vec{x}. \tag{B14}$$

[1] Y. K. Kato, R. C. Myers, A. C. Gossard and D. D. Awschalom, Observation of the Spin Hall Effect in Semiconductors, Science **306**, 1910 (2004).

[2] C. Nayak, S. H. Simon, A. Stern, M. Freedman and S. D. Sarma, Non-Abelian anyons and topological quantum computation, Rev. Mod. Phys. **80**, 1083 (2008).

[3] M. Z. Hasan and C. L. Kane, Colloquium: Topological insulators, Rev. Mod. Phys. **82**, 3045 (2010).

[4] V. Galitski and I. B. Spielman, Spin-orbit coupling in quantum gases, Nature **494**, 49 (2013).

[5] H. Zhai, Degenerate quantum gases with spin-orbit coupling: a review, Rep. Prog. Phys. **78**, 026001 (2015).

[6] J. Dalibard, F. Gerbier, G. Juzeliunas, and P. Öhberg, Colloquium: Artificial gauge potentials for neutral atoms, Rev. Mod. Phys. **83**, 1523 (2011).

[7] Y.-J. Lin, K. Jimènez-Garcìa, and I. B. Spielman, Spin-orbit-coupled Bose-Einstein condensates, Nature (London) **471**, 83 (2011).

[8] P. Wang, Z.-Q. Yu, Z. Fu, J. Miao, L. Huang, S. Chai, H. Zhai and J. Zhang, Spin-Orbit Coupled Degenerate Fermi Gases, Phys. Rev. Lett. **109**, 095301 (2012).

[9] H. Zhai, Spin-Orbit Coupled Quantum Gases, Int. J. Mod. Phys. B **26**, 1230001 (2012).

[10] L. W. Cheuk, A. T. Sommer, Z. Hadzibabic, T. Yefsah, W. S. Bakr and M. W. Zwierlein, Spin-Injection Spectroscopy of a Spin-Orbit Coupled Fermi Gas, Phys. Rev. Lett. **109**, 095302 (2012).

[11] R. A. Williams, M. C. Beeler, L. J. LeBlanc, K. Jiménez-García, and I. B. Spielman, Raman-Induced Interactions in a Single-Component Fermi Gas Near an s-Wave Feshbach Resonance, Phys. Rev. Lett. **111**, 095301 (2013).

[12] C. Qu, C. Hamner, M. Gong, C. Zhang and P. Engels, Observation of Zitterbewegung in a spin-orbit-coupled Bose-Einstein condensate, Phys. Rev. A **88**, 021604 (2013).

[13] N. Goldman, G. Juzeliunas, P. Öhberg and I. B. Spielman, Light-induced gauge fields for ultracold atoms, Rep. Prog. Phys. **77**, 126401 (2014).

[14] Z. Fu, L. Huang, Z. Meng, P. Wang, L. Zhang, S. Zhang, H. Zhai, P. Zhang and J. Zhang, Production of Feshbach molecules induced by spin-orbit coupling in Fermi gases, Nat. Phys. **10**, 110 (2014).

[15] A. J. Olson, S.-J. Wang, R. J. Niffenegger, C.-H. Li, C. H. Greene and Y. P. Chen, Tunable Landau-Zener transitions in a spin-orbit-coupled Bose-Einstein condensate, Phys. Rev. A **90**, 013616 (2014).

[16] W. S. Cole, S. Zhang, A. Paramekanti and N. Trivedi, Bose-Hubbard Models with Synthetic Spin-Orbit Coupling: Mott Insulators, Spin Textures, and Superfluidity, Phys. Rev. Lett. **109**, 085302 (2012).

[17] J. Radić, A. Di Ciolo, K. Sun and V. Galitski, Exotic quantum spin models in spin-orbit-coupled Mott insulators, Phys. Rev. Lett. **109**, 085303 (2012).

[18] J. Ruhman, E. Berg and E. Altman, Topological States in a One-Dimensional Fermi Gas with Attractive Interaction, Phys. Rev. Lett. **114**, 100401 (2015).

[19] L. Zhang, Y. Deng and P. Zhang, Scattering and effective interactions of ultracold atoms with spin-orbit coupling, Phys. Rev. A **87**, 053626 (2013).

[20] Q. Guan, X. Y. Yin, S. E. Gharashi and D. Blume, Energy spectrum of a harmonically trapped two-atom system with spin-orbit coupling, J. Phys. B **47**, 161001 (2014).

[21] X. Cui and T.-L. Ho, Spin-orbit-coupled one-dimensional Fermi gases with infinite repulsion, Phys. Rev. A **89**, 013629 (2014).

[22] X. Y. Yin, S. Gopalakrishnan and D. Blume, Harmonically trapped two-atom systems: Interplay of short-range s-wave interaction and spin-orbit coupling, Phys. Rev. A **89**, 033606 (2014).

[23] S.-J. Wang and C. H. Greene, General formalism for ultracold scattering with isotropic spin-orbit coupling, Phys. Rev. A **91**, 022706 (2015).

[24] C. D. Schillaci and T. C. Luu, Energy spectra of two interacting fermions with spin-orbit coupling in a harmonic trap, Phys. Rev. A **91**, 043606 (2015).

[25] S. Will, T. Best, U. Schneider, L. Hackermüller, D.-S. Lühmann and I. Bloch, Time-resolved observation of

coherent multi-body interactions in quantum phase revivals, Nature (London) **465**, 197 (2010).

[26] F. Serwane, G. Zürn, T. Lompe, T. B. Ottenstein, A. N. Wenz and S. Jochim, Deterministic Preparation of a Tunable Few-Fermion System, Science **332**, 336 (2011).

[27] C. Chin, R. Grimm and P. Julienne and E. Tiesinga, Feshbach resonances in ultracold gases, Rev. Mod. Phys. **82**, 1225 (2010).

[28] F. Dalfovo, S. Giorgini, L. P. Pitaevskii and S. Stringari, Theory of Bose-Einstein condensation in trapped gases, Rev. Mod. Phys. **71**, 463 (1999).

[29] T. Busch, B.-G. Englert, K. Rzążewski, and M. Wilkens, Two Cold Atoms in a Harmonic Trap, Found. Phys. **28**, 549 (1998).

[30] M. Olshanii, Atomic Scattering in the Presence of an External Confinement and a Gas of Impenetrable Bosons, Phys. Rev. Lett. **81**, 938 (1998).

[31] M. D. Girardeau, E. M. Wright and J. M. Triscari, Ground-state properties of a one-dimensional system of hard-core bosons in a harmonic trap, Phys. Rev. A **63**, 033601 (2001).

[32] B. Borca, D. Blume and C. H. Greene, A two-atom picture of coherent atom-molecule quantum beats, New J. Phys. **5**, 111 (2003).

[33] Z. Idziaszek and T. Calarco, Two atoms in an anisotropic harmonic trap, Phys. Rev. A **71**, 050701 (2005).

[34] Z. Idziaszek and T. Calarco, Analytical solutions for the dynamics of two trapped interacting ultracold atoms, Phys. Rev. A **74**, 022712 (2006).

[35] E. Braaten and H.-W. Hammer, Universality in few-body systems with large scattering length, Phys. Rep. **428**, 259 (2006).

[36] J. P. Kestner and L.-M. Duan, Level crossing in the three-body problem for strongly interacting fermions in a harmonic trap, Phys. Rev. A **76**, 033611 (2007).

[37] J. von Stecher, C. H. Greene and D. Blume, BEC-BCS crossover of a trapped two-component Fermi gas with unequal masses, Phys. Rev. A **76**, 053613 (2007).

[38] I. Stetcu, B. R. Barrett, U. van Kolck and J. P. Vary, Effective theory for trapped few-fermion systems, Phys. Rev. A **76**, 063613 (2007).

[39] D. Blume, Few-body physics with ultracold atomic and molecular systems in traps, Rep. Prog. Phys. **75**, 046401 (2012).

[40] S. E. Gharashi, K. M. Daily and D. Blume, Three s-wave-interacting fermions under anisotropic harmonic confinement: Dimensional crossover of energetics and virial coefficients, Phys. Rev. A **86**, 042702 (2012).

[41] S. E. Gharashi and D. Blume, Correlations of the Upper Branch of 1D Harmonically Trapped Two-Component Fermi Gases, Phys. Rev. Lett. **111**, 045302 (2013).

[42] A. G. Sykes, J. P. Corson, J. P. D'Incao, A. P. Koller, C. H. Greene, A. M. Rey, K. R. A. Hazzard and J. L. Bohn, Quenching to unitarity: Quantum dynamics in a three-dimensional Bose gas, Phys. Rev. A **89**, 021601 (2014).

[43] E. Fermi, Sopra lo Spostamento per Pressione delle Righe Elevate delle Serie Spettrali, Nuovo Cimento **11**, 157 (1934).

[44] K. Huang and C. N. Yang, Quantum-Mechanical Many-Body Problem with Hard-Sphere Interaction, Phys. Rev. **105**, 767 (1957).

[45] K. Huang, *Statistical Mechanics*, 2nd ed. (Wiley, Newy York, 1987).

[46] J. Hubbard, Electron Correlations in Narrow Energy Bands, Proc. Roy. Soc. (London) Ser. A **276**, 238 (1963).

[47] M. Born and R. Oppenheimer, Zur Quantentheorie der Molekeln, Ann. Phys. **389**, 457 (1927).

[48] E. Ising, Beitrag zur Theorie des Ferromagnetismus, Z. Phys. **31**, 253 (1925).

[49] W. Heisenberg, Zur Theorie des Ferromagnetismus, Z. Phys. **49**, 619 (1928).

[50] J. H. Van Vleck, On σ-Type Doubling and Electron Spin in the Spectra of Diatomic Molecules, Phys. Rev. **33**, 467 (1929).

[51] T. Kato, On the Convergence of the Perturbation Method. I, Prog. Theor. Phys. **4**, 514 (1949).

[52] P.-O. Löwdin, A Note on the Quantum-Mechanical Perturbation Theory, J. Chem. Phys. **19**, 1396 (1951).

[53] D. J. Klein, Degenerate perturbation theory, J. Chem. Phys. **61**, 786 (1974).

[54] C. E. Soliverez, General theory of effective Hamiltonians, Phys. Rev. A **24**, 4 (1981).

[55] A. L. Chernyshev, D. Galanakis, P. Phillips, A. V. Rozhkov and A.-M. S. Tremblay, Higher order corrections to effective low-energy theories for strongly correlated electron systems, Phys. Rev. B **70**, 235111 (2004).

[56] J. Levinsen, P. Massignan, G. M. Bruun, M. M. Parish, Strong-coupling ansatz for the one-dimensional Fermi gas in a harmonic potential, arXiv: 1408.7096 (2014); accepted for publication in Science Advances.

[57] F. Deuretzbacher, D. Becker, J. Bjerlin, S. M. Reimann and L. Santos, Quantum magnetism without lattices in strongly interacting one-dimensional spinor gases, Phys. Rev. A **90**, 013611 (2014).

[58] L. Yang, L. Guan and H. Pu, Strongly interacting quantum gases in one-dimensional traps, Phys. Rev. A **91**, 043634 (2015).

[59] A. G. Volosniev, D. Petrosyan, M. Valiente, D. V. Fedorov, A. S. Jensen and N. T. Zinner, Engineering the dynamics of effective spin-chain models for strongly interacting atomic gases, Phys. Rev. A **91**, 023620 (2015).

[60] I. Dzyaloshinskii, A thermodynamic theory of "weak" ferromagnetism of antiferromagnetics, J. Phys. Chem. Solids **4**, 241 (1958).

[61] T. Moriya, Anisotropic Superexchange Interaction and Weak Ferromagnetism, Phys. Rev. **120**, 91 (1960).

[62] F. Keffer, Moriya Interaction and the Problem of the Spin Arrangements in βMnS, Phys. Rev. **126**, 896 (1962).

[63] M. D. Girardeau, Relationship between Systems of Impenetrable Bosons and Fermions in One Dimension, J. Math. Phys. **1**, 516 (1960).

[64] M. D. Girardeaua, H. Nguyenb and M. Olshaniib, Effective interactions, Fermi-Bose duality, and ground states of ultracold atomic vapors in tight de Broglie waveguides, Opt. Commun. **243**, 3 (2004).

[65] E. E. Edwards, S. Korenblit, K. Kim, R. Islam, M.-S. Chang, J. K. Freericks, G.-D. Lin, L.-M. Duan and C. Monroe, Quantum simulation and phase diagram of the transverse-field Ising model with three atomic spins, Phys. Rev. B **82**, 060412(R) (2010).

[66] G.-D. Lin, C. Monroe and L.-M. Duan, Sharp Phase Transitions in a Small Frustrated Network of Trapped Ion Spins, Phys. Rev. Lett. **106**, 230402 (2011).

[67] K. Kim, M.-S. Chang, S. Korenblit, R. Islam, E. E. Edwards, J. K. Freericks, G.-D. Lin, L.-M. Duan and C. Monroe, Quantum simulation of frustrated Ising spins with trapped ions, Nature **465**, 590 (2010).

[68] J. W. Britton, B. C. Sawyer, A. C. Keith, C.-C. J.

Wang, J. K. Freericks, H. Uys, M. J. Biercuk and J. J. Bollinger, Engineered two-dimensional Ising interactions in a trapped-ion quantum simulator with hundreds of spins, Nature **484**,489 (2012).

[69] T. Zibold, E. Nicklas, C. Gross and M. K. Oberthaler, Classical Bifurcation at the Transition from Rabi to Josephson Dynamics, Phys. Rev. Lett. **105**, 204101 (2010).

[70] X. Zhang, M. Bishof, S. L. Bromley, C. V. Kraus, M. S. Safronova, P. Zoller A. M. Rey and J. Ye, Spectroscopic observation of SU(N)-symmetric interactions in Sr orbital magnetism, Science **345**, 1467 (2014).

[71] G. J. Lapeyre Jr., M. D. Girardeau and E. M. Wright, Momentum distribution for a one-dimensional trapped gas of hard-core bosons, Phys. Rev. A **66**, 023606 (2002).

[72] G. B. Arfken and H. J. Weber, *Mathematical Methods for Physics*, 6th ed. (Elsevier Acad. Press, 2008).

[73] E. Feldheim, Relations entre les polynomials de Jacobi, Laguerre et Hermite, Acta Mathematica **75**, 117 (1943).

[74] W. Magnus, F. Oberhettinger and R. P. Soni, *Formulas and Theorems for the Special Functions of Mathematical Physics*, 3rd ed. (Springer-Verlag, 1966).